The Forgotten Eleventh System: Separating Laplace's Equation in Confocal Paraboloidal Coordinates

L. D. Musa

ORCID: 0009-0000-1545-8573
DOI: 10.5281/zenodo.24532481 (Zenodo, version 4, 2026)
all versions: 10.5281/zenodo.24404423

November 25, 2026

Abstract

This note is a careful, checked guide to confocal paraboloidal coordinates for physicists. We use the notation (μ, ν, λ) of Moon and Spencer's *Field Theory Handbook*. Our contribution is not new theory. It is (i) a comparison of the Moon–Spencer and Morse–Feshbach coordinate conventions, with explicit dictionaries between them; and (ii) a set of verified corrections and clarifications. The main correction is to the printed Laplacian prefactor on p. 45 of the handbook, a misprint that persists in the corrected third printing (Springer, 1988). The coordinate, operator and separation identities were checked symbolically with `sympy`. We cover the geometry of the coordinate surfaces, the scale factors (local length factors) and vector operators, and the separation of Laplace's and Helmholtz's equations. The separated equations share two separation constants, α_2 and α_3, and agree with the handbook's Table 1.11. We analyze the degenerate symmetry planes and the parity conditions they impose. As a worked example we solve the potential between two confocal paraboloidal electrodes exactly and give the signed surface charge. A second example, following Arscott, has both separation constants nonzero: the separated equations become Mathieu equations, and smoothness and a grounded boundary together fix the two constants. A third example treats the unbounded region outside one paraboloid. For the paraboloid of revolution we also derive the far-field decay of the potential, and we give an asymptotic argument, with numerical evidence, that the same law holds for the elliptic case. Appendix A introduces Stäckel's separability theory; Appendix B identifies the system with Type IV_2 in Eisenhart's 1934 classification; Appendix C gives the proof of the far-field law.

1 Introduction

Laplace's and Helmholtz's equations separate (reduce to one ordinary differential equation for each coordinate; Sec. 4) in only a handful of three-dimensional orthogonal coordinate systems (systems whose three families of coordinate surfaces cross at right angles). The most general families are the confocal ellipsoidal coordinates and their limiting case, the confocal paraboloidal coordinates [1, 2]. In the paraboloidal system, two families of coordinate surfaces are elliptic paraboloids opening in opposite directions and the third consists of hyperbolic paraboloids, so the system is the natural one for boundary-value problems on paraboloidal surfaces, such as the potential and field near a single conducting paraboloid, obtained with both separation constants zero [9]. Unlike parabolic-cylinder or rotational parabolic coordinates, the system has no translational or rotational symmetry. Its three separated equations are coupled through two common *separation constants* (constants

introduced when a partial differential equation is split into ordinary ones). In an eigenvalue problem the boundary conditions select the allowed constant values. Here those problems are genuinely three-dimensional.

The coordinates are tabulated in the handbook of Moon and Spencer [1]. We adopt their notation (μ, ν, λ). Willatzen and Lew Yan Voon [8] treat the same system in a later textbook. Some elementary separated solutions printed in an earlier printing were later corrected [7]. Morse and Feshbach [2] use different symbols, and sometimes the same letter for a different quantity. Table 1 lists both conventions side by side.

Arfken's second edition treats these coordinates explicitly [10, §2.17, pp. 119–120], whereas the seventh edition refers readers back to the older treatment rather than presenting it [11, p. 203]; this note collects the geometry and separation formulas for readers who have worked only with the usual cylindrical and spherical systems.[1]

Roadmap. Section 2 defines the coordinates, their ranges and their surfaces. It also explains what happens on the symmetry planes $x = 0$ and $y = 0$, where one coordinate sticks at an endpoint. Section 3 gives the scale factors and the vector operators, including the corrected Laplacian. Section 4 separates Laplace's and Helmholtz's equations into three ordinary differential equations. Section 5 opens with a short recipe for using them, then solves the field between two paraboloidal electrodes. Section 6 solves a problem with both separation constants nonzero. Section 7 treats the unbounded region outside one paraboloid: the integral-transform method is included for teaching reasons, following Darai and Arscott, and for the paraboloid of revolution we derive the far-field decay of the potential. Section 8 summarizes. Appendix A explains *why* the equations separate, using Stäckel's matrix. Appendix B places the system in Eisenhart's classification of all separable coordinate systems. Appendix C gives the full proof of the far-field law. The main algebraic identities and convention dictionaries have symbolic checks. The numbers in the second example are our own computations, checked by independent methods. We also say plainly where the discussion stops: which boundary-value problems are actually solved, and how far we go in finding the allowed values of the separation constants.

2 Coordinates

In cylindrical coordinates, a boundary $r = \text{const}$ is a cylinder; in spherical coordinates, a boundary $r = \text{const}$ is a sphere. The same practical idea motivates the present system: choose coordinates so that paraboloidal boundaries are surfaces on which one coordinate is constant. The three families are mutually perpendicular where the coordinates are *regular*, that is, where the three coordinate surfaces through the point are distinct and the scale factors (Sec. 3) are finite and nonzero. The name *confocal* ("sharing a focus") is explained in Sec. 2.1 below.

2.1 Definition and coordinate surfaces

Following Moon and Spencer [1, Table 1.11], let $b > c > 0$ and $(u^1, u^2, u^3) = (\mu, \nu, \lambda)$ with $\infty > \mu > b > \lambda > c > \nu > 0$.[2] The constants b, c fix the geometry and are not coordinates. The strict

[1] This comparison concerns these two editions, not a survey of all current textbooks.

[2] Ranges, transformation and surfaces as printed in Table 1.11 (p. 44) of the corrected third printing; all were checked symbolically. The restriction $\nu > 0$ confines the system to the interior $x^2/b + y^2/c < 4z$ of the paraboloid $\nu = 0$. The formulas below remain valid for $\nu < 0$, which extends the coordinates to all of space. Arfken's range [10, p. 119, (2.143)] already includes this extension: his lowest coordinate has no positive lower bound.

inequalities specify the open region (a region without its boundary) in which we first work. The Cartesian position is given by

$$x^2 = \frac{4(\mu-b)(b-\nu)(b-\lambda)}{b-c}, \qquad y^2 = \frac{4(\mu-c)(c-\nu)(\lambda-c)}{b-c}, \qquad z = \mu+\nu+\lambda-b-c. \tag{1}$$

A useful alternative is to start with a point (x, y, z) and solve for a variable σ. The three coordinates are the roots σ of $\frac{x^2}{b-\sigma} + \frac{y^2}{c-\sigma} = 4(z-\sigma)$, on the three allowed intervals. Holding one root fixed gives its coordinate surface:

$$\mu: \ \tfrac{x^2}{\mu-b} + \tfrac{y^2}{\mu-c} = -4(z-\mu), \qquad \nu: \ \tfrac{x^2}{b-\nu} + \tfrac{y^2}{c-\nu} = 4(z-\nu), \qquad \lambda: \ \tfrac{x^2}{b-\lambda} - \tfrac{y^2}{\lambda-c} = 4(z-\lambda), \tag{2}$$

The first two families are elliptic paraboloids (bowl-shaped surfaces with elliptical horizontal sections)[3] opening towards $-z$ and $+z$, respectively. The third family consists of hyperbolic paraboloids, or saddle-shaped surfaces (Fig. 1).[4] Arfken's earlier §2.12 [10, pp. 109–112] treats a different, rotationally symmetric parabolic system: two paraboloid families and an azimuthal angle, rather than the hyperbolic-paraboloid family present here.

Arfken notation note. In the same order as his coordinates, $(\xi_1, \xi_2, \xi_3) = 2(\nu, \lambda, \mu)$; unlike the Morse–Feshbach column, these are linear labels, not square roots. His Cartesian z is reflected, as explained in the preceding footnote.

What to notice. The symbols μ, ν, λ label surfaces, not distances along Cartesian axes. Like a spherical radius, a fixed coordinate describes an entire surface. Unlike the usual spherical system, none of the three coordinates is an azimuthal angle.

Since only x^2, y^2 are determined, each triple (μ, ν, λ) labels four points $(\pm x, \pm y, z)$. To use the coordinates, one must therefore choose the signs of x and y. Each such choice gives a coordinate *chart*: a region in which each point has exactly one set of labels and nearby points have nearby labels. There are four charts, one per sign choice, and they are mirror images of one another. They live on the four open regions $x \gtrless 0$, $y \gtrless 0$; these regions do not overlap, and their common boundaries are the planes $x = 0$ and $y = 0$, treated in Sec. 2.2.

Why "confocal", and the two focal parabolas. Every parabola has one focus. Cut any of the coordinate surfaces by the plane $y = 0$. With σ standing for its coordinate value, the surface equation gives the trace $x^2 = 4(b-\sigma)(z-\sigma)$: a parabola with vertex at height $z = \sigma$ and focus at height $\sigma + (b-\sigma) = b$. The focus does not depend on σ, so every trace in this plane, from all three families, has the same focus, the point $(0, 0, b)$. In the plane $x = 0$ the traces $y^2 = 4(c-\sigma)(z-\sigma)$ likewise all have the focus $(0, 0, c)$. This shared focus is what *confocal* refers to, just as confocal ellipses in a plane share their two foci. Figure 3 shows both planes.

[3] We follow Moon and Spencer [1]. Morse and Feshbach [2, Part I, p. 664, item XI] use square-root coordinates (ξ_1, ξ_2, ξ_3) and constants $a > b$, with $x^2 = \prod_n(\xi_n^2 - a^2)/(a^2-b^2)$, $y^2 = \prod_n(\xi_n^2 - b^2)/(b^2-a^2)$, $z = \frac{1}{2}(\xi_1^2+\xi_2^2+\xi_3^2-a^2-b^2)$. These coincide with ours under $\xi_1^2 = 2\mu$, $\xi_2^2 = 2\lambda$, $\xi_3^2 = 2\nu$, $a^2 = 2b$, $b_{\mathrm{MF}}^2 = 2c$. The z axis is the same, with no sign flip and no extra factor. Beware: their b is not our b; their second coordinate ξ_2 is the hyperbolic-paraboloid one, our λ; and the parameters λ, μ, ν of their elliptic-function parametrization are unrelated to ours (their $\lambda \leftrightarrow$ our μ, their $\nu \leftrightarrow$ our λ, their $\mu \leftrightarrow$ our ν). Some handbook entries print $x^2/(a^2-\sigma) + y^2/(b^2-\sigma) = z - \sigma$, which is not an orthogonal family.

[4] Arfken [10, §2.17, pp. 119–120, (2.140)–(2.145)] uses linear coordinates $(\xi_1, \xi_2, \xi_3) = (2\nu, 2\lambda, 2\mu)$ and parameters $a_{\mathrm{A}}^2 = 2b$, $b_{\mathrm{A}}^2 = 2c$. On matching sign charts, $x_{\mathrm{A}} = x$, $y_{\mathrm{A}} = y$, but $z_{\mathrm{A}} = -z$: the axial direction is reversed, with no Cartesian dilation. His scale factors are $(h_1, h_2, h_3) = (h_\nu, h_\lambda, h_\mu)/2$ because $d\xi_i = 2\, d\sigma_i$. Thus his first family opens towards $-z_{\mathrm{A}}$, while our corresponding ν family opens towards $+z$. These ξ_i are not the square-root coordinates of Morse and Feshbach.

Table 1: Notation. Middle column: Moon and Spencer [1], used throughout. Right: the Morse–Feshbach [2, p. 664] equivalent. Here σ stands for any of μ, ν, λ. The constant dictionary combines the printed matrix on p. 664 with the separated-equation convention on p. 656. Arfken uses a different ξ_i convention, summarized below.

Quantity	Moon–Spencer (this note)	Morse–Feshbach
parameters	$b > c > 0$	$a > b$, with $a^2 = 2b$, $b_{\mathrm{MF}}^2 = 2c$ (their $b \neq$ our b)
downward paraboloids	$\mu \in (b, \infty)$	$\xi_1 = \sqrt{2\mu}$
upward paraboloids	$\nu \in (0, c)$	$\xi_3 = \sqrt{2\nu}$
hyperbolic paraboloids	$\lambda \in (c, b)$	$\xi_2 = \sqrt{2\lambda}$
z axis	$z = \mu + \nu + \lambda - b - c$	same axis, no sign flip
scale factors	$h_\mu^2 = \dfrac{(\mu-\nu)(\mu-\lambda)}{(\mu-b)(\mu-c)}$, etc. (Sec. 3; the factor that turns a small change of a coordinate into a physical length)	$h_{\xi_n} = \xi_n h_{\sigma_n}$
separation constants	α_2, α_3 (Sec. 4); Helmholtz $\kappa^2 = k^2$	k_2^2, k_3^2; $k_1^2 = k^2$; dictionary in Appendix A
symbols λ, μ, ν	the coordinates	elliptic-function parameters, unrelated to ours

The phrase *focal parabola* does not mean a parabola that has a focus, since every parabola has one. It is the traditional name for two particular curves of the system, the paraboloidal counterparts of the focal ellipse and focal hyperbola of ellipsoidal coordinates. They appear when a surface is pushed to the end of its range. As σ approaches b, the term $x^2/(b-\sigma)$ forces $x \to 0$, and the surface flattens onto a region of the plane $x = 0$ whose edge is the parabola

$$x = 0, \qquad y^2 = -4(b-c)(z-b) \qquad (\lambda = \mu = b).$$

As σ approaches c the surface flattens onto the plane $y = 0$, with edge

$$y = 0, \qquad x^2 = 4(b-c)(z-c) \qquad (\lambda = \nu = c).$$

These two edge curves are the focal parabolas, drawn dashed in Fig. 2. The first opens downward from its vertex $(0, 0, b)$, the second upward from its vertex $(0, 0, c)$, so each has its vertex at the shared focus of the other plane. On a focal parabola two coordinates are equal, as indicated in parentheses, so the coordinates are not regular there. The focal parabolas are not physical objects. They matter because they divide each symmetry plane into the pieces on which different coordinates reach the ends of their ranges (Sec. 2.2).

Check it yourself. Starting from (1), verify the surface equation $x^2/(b-\sigma) + y^2/(c-\sigma) = 4(z-\sigma)$ for each $\sigma = \mu, \nu, \lambda$. Then, on a chart with $x, y \neq 0$, calculate the coefficient of $d\nu^2$ in $ds^2 = dx^2 + dy^2 + dz^2$ and check that the mixed metric coefficient $g_{\nu\lambda}$ vanishes. *Hint and answer:* write $X = x^2$, $Y = y^2$ and use $g_{ij} = (\partial_i X)(\partial_j X)/(4X) + (\partial_i Y)(\partial_j Y)/(4Y) + (\partial_i z)(\partial_j z)$. Substitution gives $h_\nu^2 = g_{\nu\nu} = (\mu-\nu)(\lambda-\nu)/[(b-\nu)(c-\nu)]$ and $g_{\nu\lambda} = 0$. The same calculation gives the other scale factors in Sec. 3; no field equation is needed for this geometric check.

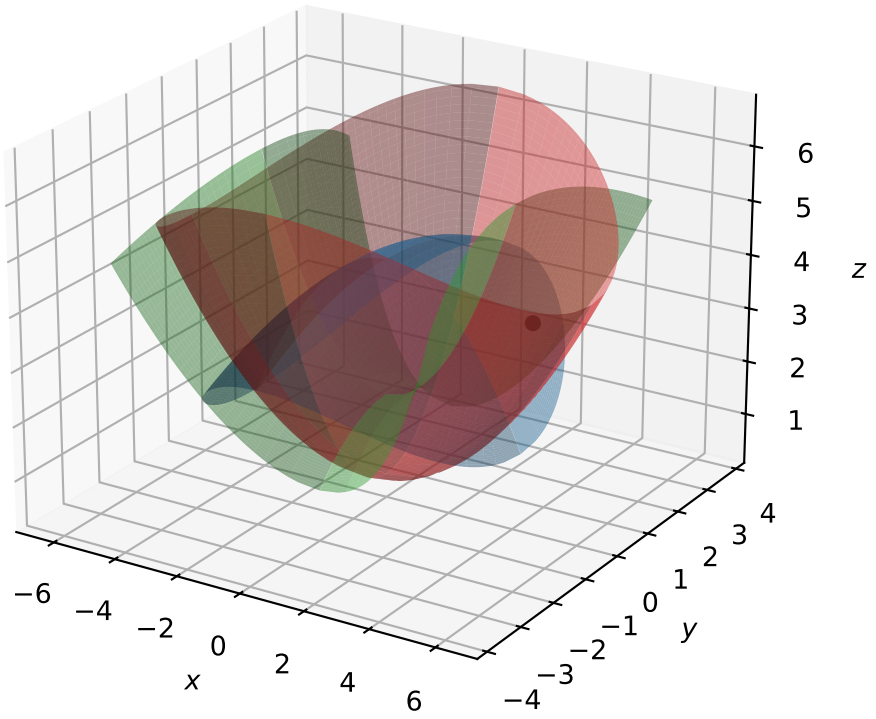


Figure 1: Coordinate surfaces for $b = 3$, $c = 1$: $\mu = 4.5$ (blue, elliptic paraboloid opening towards $-z$), $\nu = 0.5$ (red, elliptic paraboloid opening towards $+z$) and $\lambda = 2$ (green, hyperbolic paraboloid). All three are drawn only within Moon and Spencer's ranges ($0 < \nu < c$, $c < \lambda < b$, $b < \mu \leq 7$), mirrored into the four sign quadrants of (x, y), so each is a finite patch. The dot marks their intersection $(x, y, z) \approx (2.74, 1.87, 3)$.

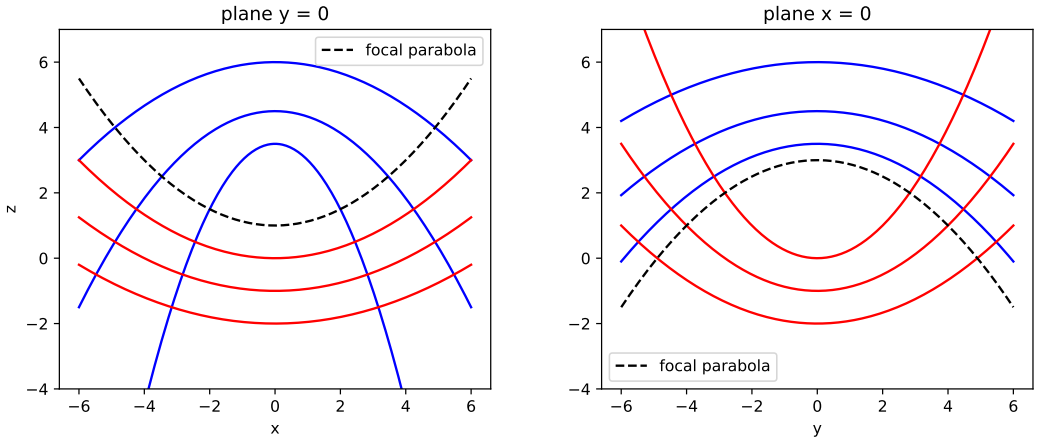


Figure 2: Traces in $y = 0$ and $x = 0$ (blue: μ, red: ν; dashed: focal parabola).

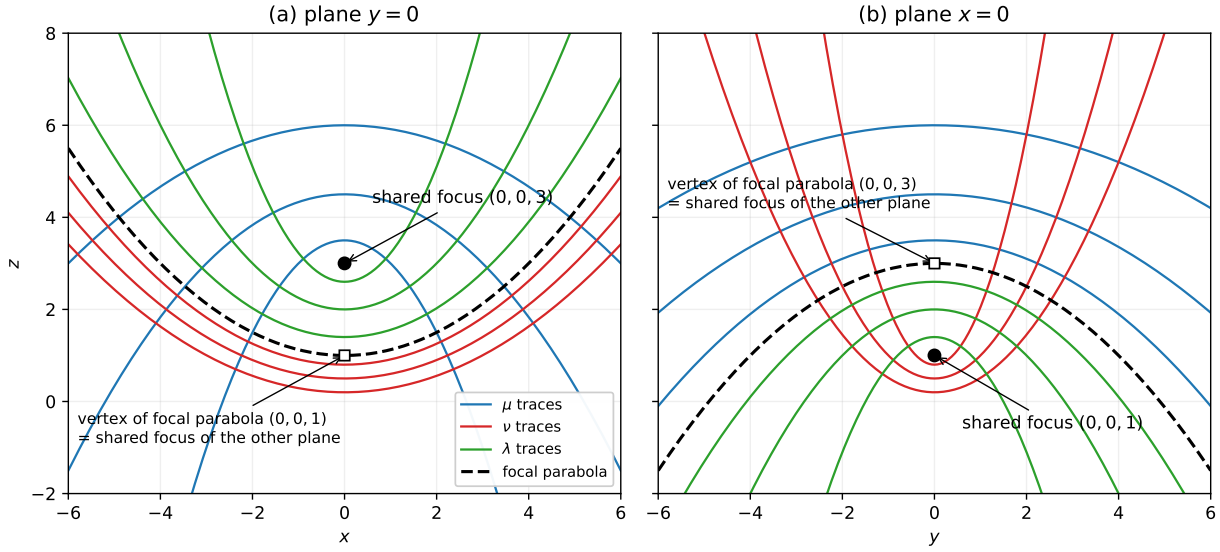


Figure 3: Why the system is called confocal, for $b = 3$, $c = 1$. (a) In the plane $y = 0$, traces of all three families of coordinate surfaces ($\mu = 3.5, 4.5, 6$; $\nu = 0.2, 0.5, 0.8$; $\lambda = 1.4, 2, 2.6$) are parabolas with one shared focus, the dot at $(0, 0, b)$. (b) In the plane $x = 0$ the shared focus is $(0, 0, c)$. The dashed curve in each panel is that plane's focal parabola, the edge onto which a surface flattens at the end of its range. Its vertex (open square) lies at the shared focus of the other plane.

2.2 Symmetry planes, degeneracies and parity

At the edges of the coordinate intervals, a surface can flatten into part of a plane. A coordinate surface is called *degenerate* when it has flattened into part of a plane or a curve. On the flattened part of a plane one coordinate sits at the end of its range, and on a focal parabola, the curve along its edge, two coordinates coincide. This is a coordinate degeneracy: the physical space remains ordinary Euclidean space, but the labels or their scale factors cease to be regular. A familiar analogy is the failure of the spherical azimuthal angle to distinguish points on the polar axis.

Equation (1) shows that $x = 0$ requires $\mu = b$ or $\lambda = b$, while $y = 0$ requires $\lambda = c$ or $\nu = c$. These alternatives describe different parts of each plane. To locate them, set $\mu = b$. The two remaining roots obey $y^2/(c-\sigma) = 4(z-\sigma)$. Clearing the denominator gives a quadratic with roots λ, ν. Evaluating it at $\sigma = b$ gives $4(b-\lambda)(b-\nu) = -4(b-c)(z-z_{f,x})$, where $z_{f,x} = b - y^2/[4(b-c)]$ is the height of the focal parabola at that y. The left-hand side is positive, so this part of the plane lies below that parabola. Repeating the substitution for $\lambda = b$ gives the complementary part. The same calculation in $y = 0$ yields the full rule:

		$z < z_f$	$z > z_f$
$x = 0,$	$z_f = z_{f,x} = b - y^2/[4(b-c)]$	$\mu = b$	$\lambda = b$
$y = 0,$	$z_f = z_{f,y} = c + x^2/[4(b-c)]$	$\lambda = c$	$\nu = c$

(3)

Figure 4 shows the two regions in each plane. At $z = z_f$ two roots coincide: this is the focal parabola itself. These are boundaries between the regions of each plane covered by different endpoint charts, not boundaries of a physical conductor. In particular, do not confuse them with the trace $z = \mu - x^2/[4(\mu - b)]$ of a nondegenerate electrode $\mu = \text{const}$ in $y = 0$.

On $x = y = 0$ the confocal cubic reduces to $(\sigma - b)(\sigma - c)(\sigma - z) = 0$, so two coordinates sit at

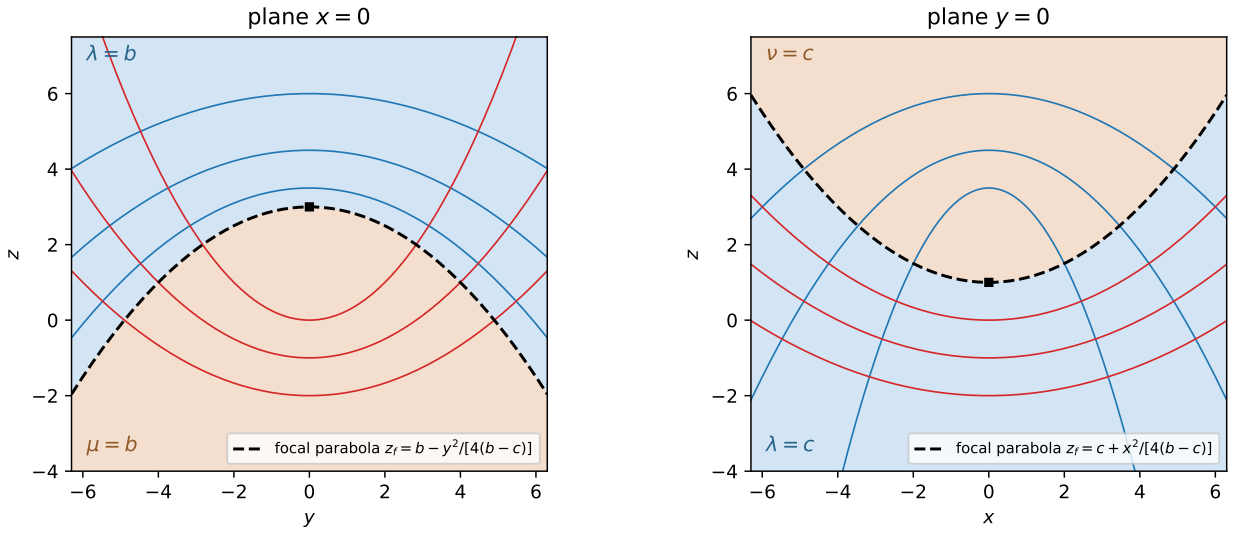


Figure 4: Degenerate coordinate planes for $b = 3, c = 1$. In $x = 0$ (left), $\lambda = b$ above the downward focal parabola and $\mu = b$ below it; in $y = 0$ (right), $\nu = c$ above the upward focal parabola and $\lambda = c$ below it. The thin blue and red curves are the same nondegenerate μ and ν traces as in Fig. 2, not the boundaries of the shading. Plotted surfaces use the extension $\nu < 0$ where stated in the text.

interval endpoints. The signs of x, y no longer distinguish charts there. This does not mean that the cubic has a repeated root at every axis point: repetition occurs at $z = b$ or $z = c$. The nominal endpoint $\nu = 0$ in the printed Moon–Spencer range is an ordinary upward elliptic paraboloid, not a symmetry plane: only with the additional limit $\lambda = c$ does it give $y = 0$, $x^2 = 4b(\mu - b)$ and $z = \mu - b$. There is no endpoint $\mu = c$, since $\mu > b > c$ throughout.

Smoothness and reflection symmetry. A coordinate singularity is a place where the coordinates fail (labels coincide, or a scale factor vanishes or diverges); it need not be a place where anything is wrong with the field. We must ask how a smooth field (one with continuous derivatives of every order) crosses $x = 0$ or $y = 0$. An even field is unchanged by the corresponding reflection; an odd field changes sign.

The factors $M(\mu), N(\nu), \Lambda(\lambda)$ introduced in Sec. 4 satisfy ordinary differential equations (ODEs). Write any one of them as $F(s)$. Near an endpoint $s_0 = b$ or c, inserting $F \sim |s - s_0|^r$ into the leading terms of its ODE (here $f \sim g$ means that $f/g \to 1$ in the limit considered, for F up to a constant factor, and $O(g)$, used below, means bounded by a constant times $|g|$ in that limit) gives $r(r - \frac{1}{2}) = 0$. This is the *indicial equation*; its roots give the leading powers of the two local solutions. Introduce a positive local square-root variable on the chosen side of the plane: $t_\mu = \sqrt{\mu - b}$, $t_{\lambda,b} = \sqrt{b - \lambda}$, $t_{\lambda,c} = \sqrt{\lambda - c}$ or $t_\nu = \sqrt{c - \nu}$. Then

$$F = A_0 + A_1 t + O(t^2), \tag{4}$$

where the even and odd powers belong to two independent local solutions (the "even branch" and the "odd branch"). The same leading powers occur for Helmholtz's equation. This conclusion follows from the handbook's ODEs; it is not a boundary prescription quoted from the handbook. Morse and Feshbach's coordinates $\xi_n = \sqrt{2\sigma_n}$ are also square roots, but they are not these local variables t, which measure distance from b or c.

For reflection across a plane, extend t with a sign chosen to follow the sign of the transverse Cartesian coordinate. The even branch has $dF/dt = 0$ at $t = 0$; the odd branch has $F = 0$ there. Explicitly:

plane	endpoint chart	Cartesian even	Cartesian odd
$x = 0$	$\mu = b$	$dM/dt_\mu\|_0 = 0$	$M(b) = 0$
$x = 0$	$\lambda = b$	$d\Lambda/dt_{\lambda,b}\|_0 = 0$	$\Lambda(b) = 0$
$y = 0$	$\lambda = c$	$d\Lambda/dt_{\lambda,c}\|_0 = 0$	$\Lambda(c) = 0$
$y = 0$	$\nu = c$	$dN/dt_\nu\|_0 = 0$	$N(c) = 0$

These derivatives are with respect to t, *not* the original coordinate s. For example, an even branch $F = A_0 + A_2 t^2 + \cdots$ generally has a nonzero derivative with respect to s. An odd branch $F = A_1 t + \cdots$ generally has a divergent s derivative, although its derivative with respect to t is finite. The square-root coordinate removes this apparent singularity.

What to notice. Local smoothness is not a complete eigenvalue problem. Equation (1) gives $x \propto t_\mu t_{\lambda,b}$ and $y \propto t_\nu t_{\lambda,c}$, explaining why each plane has two endpoint charts. At a focal parabola the limits of the field taken from the adjoining regions must also match. Arscott [13, (2.2)–(2.15)] derives these matching conditions: for a field smooth on the axis they force 2π-periodicity in his angle β, hence one integer index, while α_3 stays continuous until a boundary condition fixes it (Sec. 6). There is no parity condition for M at c, because $\mu = c$ is outside its range.

3 Scale factors and vector operators

A coordinate increment is not generally a physical distance. The positive *scale factor* h_q converts a small change dq, with the other coordinates held fixed, into distance $h_q|dq|$. This is the same role played by the familiar factors $1, r, 1$ in cylindrical coordinates. For our three coordinates the squared scale factors are

$$h_\mu^2 = \frac{(\mu-\nu)(\mu-\lambda)}{(\mu-b)(\mu-c)}, \quad h_\nu^2 = \frac{(\mu-\nu)(\lambda-\nu)}{(b-\nu)(c-\nu)}, \quad h_\lambda^2 = \frac{(\lambda-\nu)(\mu-\lambda)}{(b-\lambda)(\lambda-c)}. \tag{5}$$

The squared length of a small displacement $(d\mu, d\nu, d\lambda)$, called the squared line element, is therefore

$$ds^2 = h_\mu^2\, d\mu^2 + h_\nu^2\, d\nu^2 + h_\lambda^2\, d\lambda^2. \tag{6}$$

It has no mixed terms such as $d\mu\, d\nu$, and this means that the coordinate directions are orthogonal. The scale factors are obtained by differentiating the formulas for Cartesian position in Eq. (1); the symbolic checks also verify that the cross terms vanish.

Comparison of conventions. In the Morse–Feshbach coordinates $\xi_n = \sqrt{2\sigma_n}$ (footnote in Sec. 2) the scale factors acquire the change-of-variable factor $d\sigma/d\xi = \xi$, $h_{\xi_n} = \xi_n h_{\sigma_n}$, e.g. $h_1 = \xi_1\big[(\xi_1^2-\xi_2^2)(\xi_1^2-\xi_3^2)/((\xi_1^2-a^2)(\xi_1^2-b^2))\big]^{1/2}$ [2, p. 664]. The Laplacian there takes the form $\sum_n h_n^{-2} f_n^{-1} \partial_{\xi_n}(f_n \partial_{\xi_n})$ with $f_n = \xi_n^{-1}\sqrt{(\xi_n^2-a^2)(\xi_n^2-b^2)}$, which gives the same differential expression after the change of variables. For a real positive one-coordinate factor, take $f_n = \xi_n^{-1}\sqrt{|(\xi_n^2-a^2)(\xi_n^2-b^2)|}$. The printed square root, continued as a complex function, differs from the positive real square root by a constant factor of unit size (here $\pm i$, because the quantity under the root is negative on the middle interval); this factor cancels from $f_n^{-1}\partial_{\xi_n}(f_n\partial_{\xi_n})$. In that representation the singular points (where the coefficient of the highest derivative vanishes,

once denominators are cleared) are $\xi = 0, \pm a, \pm b$ rather than $s = b, c$ in the unified equation. Some of these points lie outside the allowed coordinate intervals.

The coefficients of ds^2 in Eq. (6) form the *metric tensor* $g_{qq'}$ of the coordinate system, the rule that turns small coordinate changes into squared length. Here it is diagonal, with $g_{qq} = h_q^2$ and all off-diagonal components zero. (The metric tensor is not the same as the metric of a metric space, a distance function between two points that satisfies three axioms; the two are linked, since the length of the shortest path measured with ds is such a distance.) Appendix A explains how Moon and Spencer encode it in a Stäckel matrix and why that helps separation.

Let $\mathbf{r} = (x, y, z)$ and $\partial_q = \partial/\partial q$. The vector $\mathbf{e}_q = h_q^{-1}\partial_q \mathbf{r}$ has unit length and points in the direction of increasing q. Put $H = h_\mu h_\nu h_\lambda$, the factor converting a coordinate volume into physical volume. If $F_q = \mathbf{F} \cdot \mathbf{e}_q$ denotes a physical vector component, the usual orthogonal-coordinate formulas give the gradient, divergence and curl below. Orientation matters for curl: the triad $(\mathbf{e}_\mu, \mathbf{e}_\lambda, \mathbf{e}_\nu)$ is right-handed for $xy > 0$.[5] The displayed curl formula uses this right-handed order on a chart with $xy > 0$; it needs an overall minus sign on a chart with $xy < 0$. Gradient and divergence do not require this orientation choice.

$$\nabla f = \sum_q \frac{\mathbf{e}_q}{h_q}\partial_q f, \qquad \nabla \cdot \mathbf{F} = \frac{1}{H}\sum_q \partial_q\Big(\frac{H}{h_q}F_q\Big), \tag{7}$$

$$(\nabla \times \mathbf{F})_{q_1} = \frac{1}{h_{q_2}h_{q_3}}\big[\partial_{q_2}(h_{q_3}F_{q_3}) - \partial_{q_3}(h_{q_2}F_{q_2})\big], \quad (q_1, q_2, q_3) \text{ cyclic in } (\mu, \lambda, \nu), \tag{8}$$

The Laplacian is the divergence of the gradient. Combining the first two formulas gives the following real expression, valid on each regular chart (a chart whose points all have $b < \mu$, $c < \lambda < b$, $0 < \nu < c$ strictly):

$$\nabla^2 u = \sum_{s \in \{\mu,\nu,\lambda\}} \frac{(s-b)(s-c)\,\partial_s^2 u + \frac{1}{2}(2s-b-c)\,\partial_s u}{\prod_{q \neq s}(s-q)}. \tag{9}$$

Here s runs over μ, ν, λ; the product in the denominator contains the two other coordinates. The scalar symbols f and u above denote arbitrary fields. In electrostatics u will denote the potential.

What to notice. The operator has the same purpose as the spherical or cylindrical Laplacian; only its geometric coefficients have changed. Its particularly symmetric form is useful: the same differential expression occurs once for each coordinate. That repeated structure is the starting point for separation.

[5] The scale factors, gradient and divergence agree term by term with Moon and Spencer [1, Table 1.11, pp. 44–45]. Their matrix, determinant and one-coordinate factors also agree; these are defined and checked in Appendix A. Their curl is written as a determinant in the order (μ, ν, λ), which is right-handed only where $xy < 0$; where $xy > 0$ it gives $-\nabla \times \mathbf{E}$. The handedness of any ordering flips between adjacent quadrants, because only x^2, y^2 are fixed. The same ordering is used by Willatzen and Lew Yan Voon [8, Eq. (17.9)]. The Laplacian misprint on p. 45 of the second edition persists in the corrected third printing (Springer, 1988) consulted for this note. It carries the exponent $\frac{1}{2}$ on the whole ratio $[(s-b)(s-c)/\prod_{q\neq s}(s-q)]^{1/2}$. That form is inconsistent with the same page's g_{ii} and one-coordinate factors f_i, is dimensionally inconsistent, and differs from $\nabla\cdot\nabla$ built from their own grad and div; the square root must cover the numerator only, with the signs of the real square roots chosen for each interval. The expanded real formula below avoids that ambiguity. The persistence of this form in the corrected third printing was confirmed by visual inspection of a photograph of that printing on 7 November 2026; the printing checked is identified in Ref. [1]. The Laplacian printed in Willatzen and Lew Yan Voon [8, Eq. (17.10)] and in Duggen, Willatzen and Lew Yan Voon [9, Eq. (7)] contains the same typographical slip; the correct form is the one used here, with the square root covering the numerator only.

4 Separation

Separation replaces a partial differential equation (PDE), involving several coordinates, by ODEs involving one coordinate each. Start with one product $\psi = M(\mu)N(\nu)\Lambda(\lambda)$. This is an ansatz: we seek solutions of that form, without assuming that every field is one product. As with spherical harmonics or cylindrical modes, more general boundary data may require superpositions, meaning sums of separated product solutions.

Substitute the product into the Laplacian of Sec. 3 and divide by the product on a region where it is nonzero. Each numerator now contains derivatives of only its own factor. The denominators still involve all three coordinates, so independence of the coordinates alone is not the whole argument. The cancellation identities stated below, or equivalently the Stäckel calculation in Appendix A, finish the separation. The resulting equations are those printed by Moon and Spencer [1, Table 1.11, p. 46]:

$$(\mu - b)(\mu - c)M'' + \tfrac{1}{2}[2\mu - (b + c)]M' - [\alpha_2 - \alpha_3\mu]M = 0, \tag{10}$$

$$(b - \nu)(c - \nu)N'' + \tfrac{1}{2}[2\nu - (b + c)]N' - [\alpha_2 - \alpha_3\nu]N = 0, \tag{11}$$

$$(b - \lambda)(\lambda - c)\Lambda'' - \tfrac{1}{2}[2\lambda - (b + c)]\Lambda' + [\alpha_2 - \alpha_3\lambda]\Lambda = 0, \tag{12}$$

Primes denote derivatives with respect to the factor's own argument: $M' = dM/d\mu$, for example. The numbers α_2, α_3 are *separation constants*: they are independent of position and must have the same values in all three equations. Their subscripts follow Moon and Spencer's convention. Boundary and smoothness conditions, not separation alone, determine which values are appropriate.

All three ODEs are the single equation $(s - b)(s - c)F'' + \frac{1}{2}(2s - b - c)F' + (\alpha_3 s - \alpha_2)F = 0$ written on the three intervals; the λ equation is multiplied by -1 so that its leading coefficient is positive. The cancellation uses the identities

$$\sum_{i=1}^{3} \frac{q_i^m}{\prod_{j\neq i}(q_i - q_j)} = \begin{cases} 0, & m = 0, 1, \\ 1, & m = 2, \end{cases} \qquad (q_1, q_2, q_3) = (\mu, \nu, \lambda). \tag{13}$$

The index m here is an integer power, not a wave number. Thus constant and linear numerator terms cancel when the three coordinate contributions are added. A quadratic term does not cancel: it produces a constant in the original PDE. Appendix A derives this mechanism from a matrix rather than requiring the reader to guess it.

Source comparison (optional on a first reading). Morse and Feshbach [2, pp. 655–656, 664] use $\xi_n^2 = 2\sigma_n$, with $(\sigma_1, \sigma_2, \sigma_3) = (\mu, \lambda, \nu)$. Their p. 656 separated equations use k_1^2, k_2^2, k_3^2, with $k_1^2 = k^2$ for Helmholtz and k_2^2, k_3^2 the separation constants. Together with the printed matrix on p. 664, this gives the verified constant dictionary in Appendix A. Their p. 665 discussion allows a prefactor, $\psi = X_1X_2X_3/R$; $R = 1$ for this system is our direct verification, not a paraboloidal claim quoted from that page.[6]

[6] Morse and Feshbach also give the separable potential $V = \sum_n u_n(\xi_n)/\prod_{j\neq n}(\xi_n^2 - \xi_j^2)$, where the u_n are arbitrary functions of one variable. This V is a potential term in a wave equation, not the electrode voltage of Sec. 5. Eisenhart [5] sets out to write this potential in Cartesian coordinates x, y, z for the ten non-Cartesian systems of his 1934 letter. He does so for eight of them. For the last two, the ellipsoidal system and this one, the coordinates x_i are the roots of a cubic equation whose coefficients depend on x, y, z. Eisenhart notes that when this cubic has three real roots it is in general "irreducible," and that it is then "impossible to find the x_i as functions of x, y, and z"; he gives instead a numerical procedure, using the trigonometric form of the roots, for particular values. (The roots can still be written explicitly by Cardano's formula, but that form then requires complex intermediate quantities; the trigonometric form avoids this.) His Stäckel expression $V = \sum_i f_i(x_i)/H_i^2$ agrees with the Morse–Feshbach form

What to notice. There are three ODEs but only two shared separation constants for Laplace's equation. They cannot be chosen independently in each factor. This is analogous to the way the same angular separation constant enters both the radial and angular equations in spherical coordinates. The endpoint conditions of Sec. 2.2 supply local smoothness information, not the full boundary-value solution.

Helmholtz equation. Here k is the prescribed wave number in $(\nabla^2+k^2)\psi = 0$. It is not another freely chosen separation constant. The quadratic identity just described supplies the needed $k^2\psi$ term. Each of the first two ODEs therefore gains $+k^2s^2F$, while the positive-leading-coefficient λ equation gains $-k^2\lambda^2\Lambda$. In unified form:

$$(s-b)(s-c)F'' + \tfrac{1}{2}(2s-b-c)F' + (k^2s^2 + \alpha_3 s - \alpha_2)F = 0. \tag{14}$$

This is exactly the general case printed by Moon and Spencer [1, Table 1.11, p. 47] with $\kappa^2 = k^2$ (their λ equation is again -1 times the unified form). Setting $k = 0$ returns Laplace's equation. The same page's specialization $\alpha_2 = (b+c)q$, $\alpha_3 = -p(p+1)$ recovers their Baer-function case on p. 48. The symbols p, q in that specialization are parameters, not coordinates. "Baer function" names a special-function solution of the resulting ODE; no additional solution formula or normalization is asserted here.

The next section uses the particularly simple choice $k = \alpha_2 = \alpha_3 = 0$. It illustrates how a boundary adapted to one coordinate can reduce the calculation to a single integration. Section 6 then treats a problem in which both constants are nonzero.

5 Example: field between two confocal paraboloids

How to use the separated equations. The following recipe summarizes Secs. 2–4 for a boundary-value problem.

1. *Fit the boundaries.* Check that each boundary is a coordinate surface μ, ν or $\lambda = \text{const}$ for one choice of $b > c > 0$ (Eq. (1) and Fig. 1).
2. *Separate.* Write $\psi = M(\mu)N(\nu)\Lambda(\lambda)$. Each factor obeys the single equation $(s-b)(s-c)F'' + \frac{1}{2}(2s-b-c)F' + (k^2s^2 + \alpha_3 s - \alpha_2)F = 0$ on its own interval (Sec. 4). Set $k = 0$ for Laplace's equation.
3. *Impose symmetry.* If the problem is even or odd under $x \to -x$ or $y \to -y$, apply the endpoint conditions at $s = b, c$ of Sec. 2.2.
4. *Impose the boundary values.* Choose α_2, α_3, and superpose solutions if needed, so the boundary conditions hold. In unbounded regions a condition at infinity is also needed for uniqueness.
5. *Compute fields.* Use the operators of Sec. 3, e.g. $\mathbf{E} = -\nabla u$.

The example below is the simplest case. Both boundaries are μ surfaces and $\alpha_2 = \alpha_3 = k = 0$, so steps 3 and 4 are trivial.

after $\xi_n^2 = 2\sigma_n$ and a redefinition of the arbitrary one-variable functions. The notation f_i, x_i, H_i in that expression is Eisenhart's. The plus sign of the middle arbitrary function in the p. 664 numerator corresponds to replacing u_2 by its negative in the product-denominator form; it does not restrict the class of potentials.

Take the region between the surfaces $\mu = \mu_1$ and $\mu = \mu_2$ ($b < \mu_1 < \mu_2$), held at potentials V_1, V_2. A solution depending on μ alone ($k = \alpha_2 = \alpha_3 = 0$) satisfies $\big(\sqrt{(\mu-b)(\mu-c)}\,u'\big)' = 0$, so

$$u = V_1 + (V_2 - V_1)\frac{G(\mu) - G(\mu_1)}{G(\mu_2) - G(\mu_1)}, \qquad G(\mu) = \ln\big[2\mu - b - c + 2\sqrt{\mu - b}\sqrt{\mu - c}\big], \tag{15}$$

as printed in [1, p. 46]. Define the signed coefficient and interval by

$$C_2 = \frac{V_2 - V_1}{\Delta G}, \qquad \Delta G = G(\mu_2) - G(\mu_1) > 0. \tag{16}$$

Then $G'(\mu) = [(\mu - b)(\mu - c)]^{-1/2}$, and

$$u'(\mu) = \frac{C_2}{\sqrt{(\mu-b)(\mu-c)}}, \qquad \mathbf{E} = -\nabla u = -\frac{\mathbf{e}_\mu}{h_\mu}u'(\mu) = -\frac{C_2}{\sqrt{(\mu-\nu)(\mu-\lambda)}}\,\mathbf{e}_\mu. \tag{17}$$

In particular,

$$|\mathbf{E}| = \frac{|C_2|}{h_\mu\sqrt{(\mu-b)(\mu-c)}} = \frac{|C_2|}{\sqrt{(\mu-\nu)(\mu-\lambda)}}. \tag{18}$$

For the stated $\mu_1 < \mu_2$, the last equality requires $\nu < \mu_1$ and $\lambda < \mu_1$, which hold in the whole field region. The electric-field direction is inward if $V_2 > V_1$ and reverses with $V_2 - V_1$.[7]

Figure 5 shows the configuration.

[7] This is the special solution $M = A + B\ln[2\mu - b - c + 2\sqrt{\mu - b}\sqrt{\mu - c}]$ for $\alpha_2 = \alpha_3 = 0$ printed in Ref. [1, Table 1.11, p. 46], together with $N = A + B\ln[b + c - 2\nu - 2\sqrt{b - \nu}\sqrt{c - \nu}]$ and $\Lambda = A + B\sin^{-1}\{[2\lambda - (b + c)]/(b - c)\}$; we verified all three. These forms agree with the replacements proposed in Ref. [7] for an earlier printing. In the variable $\xi_1 = \sqrt{2\mu}$ of Ref. [2], M reads $\ln[\xi_1^2 - \frac{1}{2}(a^2 + b^2) + \sqrt{(\xi_1^2 - a^2)(\xi_1^2 - b^2)}]$ up to a constant. Ref. [2] gives the coordinates (pp. 514–515) and the separation-table entry (p. 664) but no explicit solutions for this case. The same μ-only solution was used for a single conducting paraboloid in Ref. [9] and in Willatzen and Lew Yan Voon [8, §17.5.1].

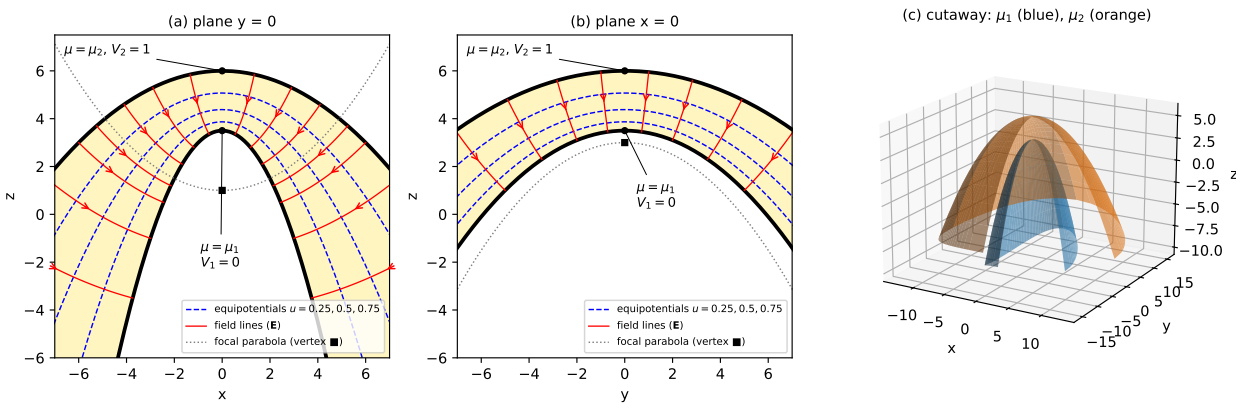


Figure 5: Geometry of the boundary-value problem for $b = 3$, $c = 1$, $\mu_1 = 3.5$, $\mu_2 = 6$, $V_1 = 0$, $V_2 = 1$. (a) Plane $y = 0$; (b) plane $x = 0$. Bold curves are the electrodes $\mu = \mu_{1,2}$, which are elliptic paraboloids opening towards $-z$; the shaded region lies between them. Dashed curves are the equipotentials $u = 0.25, 0.5, 0.75$, obtained by inverting the exact solution $u(\mu)$. Red curves are field lines, i.e. μ-coordinate curves at fixed (ν, λ), with arrows pointing along $\mathbf{E}$ from V_2 to V_1. Dotted curves are the focal parabolas, with their vertices marked by squares. (c) Cutaway view of the two electrodes. All curves are computed from Eq. (1) and the solution above, and the surfaces are drawn using the extension $\nu < 0$. Field lines and equipotentials were checked numerically to be orthogonal (max. $|\cos\theta| \approx 5 \times 10^{-6}$, the finite-difference error).

Field strength and surface charge. For conducting electrodes in vacuum, let $\mathbf{n}_i$ point *out of the conductor* and into the field region. Thus $\mathbf{n}_1 = \mathbf{e}_\mu$ on $\mu = \mu_1$ and $\mathbf{n}_2 = -\mathbf{e}_\mu$ on $\mu = \mu_2$. The conductor surface charge follows from $\sigma_i = \varepsilon_0 \mathbf{E} \cdot \mathbf{n}_i$:

$$\sigma_1(\nu, \lambda) = -\frac{\varepsilon_0 C_2}{\sqrt{(\mu_1 - \nu)(\mu_1 - \lambda)}}, \qquad \sigma_2(\nu, \lambda) = \frac{\varepsilon_0 C_2}{\sqrt{(\mu_2 - \nu)(\mu_2 - \lambda)}}. \tag{19}$$

This sign convention fixes the charge unambiguously. If $V_2 > V_1$ then $C_2 > 0$, so $\sigma_1 < 0$ and $\sigma_2 > 0$, and $\mathbf{E}$ points from μ_2 to μ_1; these signs reverse when $V_2 < V_1$. The magnitude rule $\sigma = \varepsilon_0 |\mathbf{E}|$ alone would lose this information.

The largest magnitude on either entire electrode occurs at its vertex $(x, y, z) = (0, 0, \mu_i)$, whose coordinate limit is $(\nu, \lambda) \to (c, b)$:

$$|\mathbf{E}|_{\text{vertex},i} = \frac{|C_2|}{\sqrt{(\mu_i - b)(\mu_i - c)}}, \tag{20}$$

$$\sigma_{\text{vertex},1} = -\frac{\varepsilon_0 C_2}{\sqrt{(\mu_1 - b)(\mu_1 - c)}}, \qquad \sigma_{\text{vertex},2} = \frac{\varepsilon_0 C_2}{\sqrt{(\mu_2 - b)(\mu_2 - c)}}. \tag{21}$$

It falls monotonically as ν decreases at fixed λ, and σ_i has the same spatial dependence as $|\mathbf{E}|$ apart from its sign. At fixed λ, as $\nu \to -\infty$,

$$|\mathbf{E}(\mu, \nu, \lambda)| \sim \frac{|C_2|}{\sqrt{(-\nu)(\mu - \lambda)}}. \tag{22}$$

Thus $|\mathbf{E}| = O((-\nu)^{-1/2})$ along that ray. At fixed (ν, λ), as $\mu \to \infty$, $|\mathbf{E}| \sim |C_2|/\mu$ instead, and $G(\mu) \sim \ln(4\mu)$. The potential difference between widely separated paraboloids therefore grows slowly, but the use of this unbounded coordinate continuation is distinct from imposing a uniqueness condition at infinity.

For $b = 3, c = 1, \mu_1 = 3.5, \mu_2 = 6, V_1 = 0, V_2 = 1$, numerically $\Delta G = 1.10101341877635$ and $C_2 = 0.908254143815415$. The vertex values are

$$|\mathbf{E}|_{\text{vertex},1} = 0.8123672 \text{ V/m}, \qquad |\mathbf{E}|_{\text{vertex},2} = 0.2345102 \text{ V/m}, \tag{23}$$

and there $\sigma_1/\varepsilon_0 = -0.8123672$ V/m and $\sigma_2/\varepsilon_0 = 0.2345102$ V/m. Figure 6 shows these charges along the two symmetry-plane traces. Its solid $y = 0$ curve uses $x^2 = 4(\mu_i - b)(b - \lambda)$ and $z = \mu_i + \lambda - b$, and its dashed $x = 0$ curve uses $y^2 = 4(\mu_i - c)(c - \nu)$ and $z = \mu_i + \nu - c$; these are traces of the nondegenerate electrodes, as in Fig. 5, not the chart-boundary regions of Fig. 4.

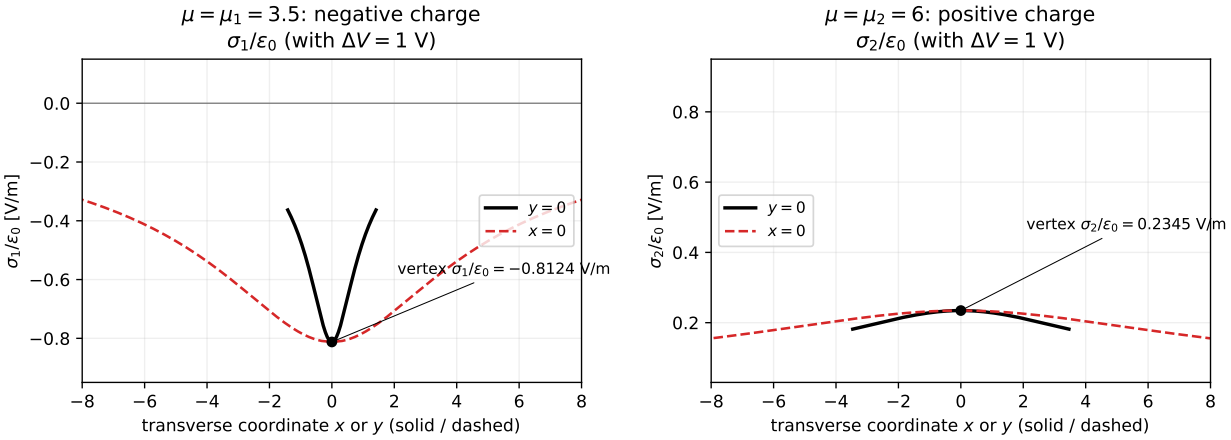


Figure 6: Signed surface charge per ε_0 for the stated numerical example, along the $y = 0$ (solid) and $x = 0$ (dashed) traces of each electrode. Both pass through the axis vertex at zero transverse coordinate. Negative on μ_1 and positive on μ_2, the density has greatest magnitude at each vertex and decreases away from it. The potential difference is 1 V, so σ_i/ε_0 has units V/m.

The symbolic gradient, the signed charge formulas and these cross-sections were checked against the formulas for Cartesian position. An independent Cartesian finite-difference gradient at 100 random interior points agreed with the coordinate expression with maximum relative error 1.92×10^{-9} for spacing 10^{-4}.

Finally, total charge and capacitance must be defined for a finite piece cut off from each electrode (a truncation), because the electrodes extend to infinity; they are not inferred from the local charge density alone. Likewise, uniqueness of the Dirichlet problem (find the potential from its values on the boundary) requires a specified condition at infinity in addition to the two electrode potentials.

6 Example: nonzero separation constants

In the example of Sec. 5, $\alpha_2 = \alpha_3 = 0$, so the three factors never interact. Here we solve a problem in which both separation constants are nonzero and the three factors must agree. We keep $b = 3$, $c = 1$ and the outer electrode $\mu = 6$ of Sec. 5 (there μ_2), now called μ_0, and take the region

$$\Omega = \{\nu > 0,\ \mu < \mu_0\}. \tag{24}$$

This is the bounded region inside the upward paraboloid $\nu = 0$, $x^2/b + y^2/c = 4z$, and below the downward paraboloid $\mu = \mu_0$. On the axis it runs from $z = 0$ to $z = \mu_0$. The paraboloid

$\mu = \mu_0$ is grounded and the potential is prescribed on $\nu = 0$. The two surfaces meet on the closed curve $\nu = 0$, $\mu = \mu_0$ (closed: it returns to its start), which runs from $(\pm 6, 0, 3)$ to $(0, \pm 2\sqrt{5}, 5)$. Arscott [13, §6] formulated and solved this boundary-value problem in his own coordinates. We follow his solution and state it in our notation.

6.1 Mathieu form of the separated equations

With $s = c + (b - c)\cos^2\theta$, the unified equation of Sec. 4 with $k = 0$ becomes Mathieu's equation

$$\frac{d^2 w}{d\theta^2} + (a - 2q\cos 2\theta)\, w = 0, \qquad a = 4\alpha_2 - 2\alpha_3(b + c), \qquad q = \alpha_3(b - c). \tag{25}$$

The same substitution appears, for the normalized interval $0 < s < 1$, in Arscott's book [15, p. 2, Eqs. (1)–(2)]. The three factors use different arguments: $\theta = i\alpha$ for M, $\theta = \beta$ for Λ and $\theta = \frac{1}{2}\pi + i\gamma$ for N, where

$$\mu = b + (b - c)\sinh^2\alpha, \qquad \lambda = c + (b - c)\cos^2\beta, \qquad \nu = c - (b - c)\sinh^2\gamma. \tag{26}$$

These (α, β, γ) are Arscott's paraboloidal coordinates. His formulas for Cartesian position [13, (1.1)] agree with Eq. (1) when his constant is $b - c$ and $(x, y, z) = (z_{\mathrm{A}},\, y_{\mathrm{A}},\, x_{\mathrm{A}} + \frac{1}{2}(b + c))$, so his axis is our z axis. His separated equations [13, (4.2)–(4.4)] are Eq. (25) with these three arguments. The pair (a, q) is only a relabeling of (α_2, α_3), and it is common to all three factors. For a given q, Mathieu's equation has solutions of period 2π only for special values of a, called characteristic values $a_n(q)$ and $b_n(q)$; those solutions are ce_n and se_n. The same functions of an imaginary argument $i\alpha$ (written Ce_n and Se_n) solve the radial equation, which is Eq. (25) with $\theta = i\alpha$. Fek_n is a second radial solution, built from modified Bessel functions K; $\mathrm{Fek}_n(\alpha, -p)$ with $p > 0$, the case used in Sec. 7, decays at large α [20, §§2.151, 8.14, 8.30, 11.12]. Boyer, Kalnins and Miller list the same single-valued product solutions, in their own coordinates and constants [16, p. 48, (2.25)], [17, (6.22)].[8]

6.2 How the coupled matching fixes the constants

Three conditions act on the one pair (α_2, α_3). Our own statement of them is as follows; the matching analysis is Arscott's [13, (2.2)–(2.15)].

1. *Single-valuedness.* The point (α, β, γ) returns to itself when β increases by 2π, so Λ must be 2π-periodic in β. This forces a to be a Mathieu characteristic value, $a = a_n(q)$ or $b_n(q)$, with integer order n. The constant q, and with it α_3, is still free [13, pp. 136–137].
2. *Smoothness across $x = 0$ and $y = 0$.* At each plane the two factors that meet there, M and Λ at $x = 0$ and Λ and N at $y = 0$, must have the same parity in the local variables of Sec. 2.2 [13, (2.12)–(2.15)]. For data even in x and y this selects the functions ce_{2n}, which are even about $\beta = 0$ and $\beta = \frac{1}{2}\pi$. Since $\mathrm{ce}_{2n}(\theta, q) = \sum_r A_{2r}^{(2n)} \cos 2r\theta$, and $\cos 2r\theta$ is a polynomial of degree r in $\cos^2\theta = (s - c)/(b - c)$, one entire function (a function given by a convergent power series for every value of s)

$$F(s) = \sum_{r \geq 0} A_{2r}^{(2n)}\, T_r\!\left(\frac{2(s - c)}{b - c} - 1\right), \tag{27}$$

[8] In Miller's Table 14, system 9, the constant c is our $b - c$ and $(x, y, z) = (y_{\mathrm{M}},\, x_{\mathrm{M}},\, z_{\mathrm{M}} + \frac{1}{2}(b + c))$. The same correspondence holds for the coordinates in [16, Table 1]. We checked this correspondence symbolically.

where T_r is a Chebyshev polynomial, serves as M, Λ and N on all three intervals. The product $F(\mu)F(\nu)F(\lambda)$ is then a symmetric function of the three roots of the cubic in Sec. 2. It is therefore an analytic function of (x, y, z) (given by a convergent power series about every point, hence smooth), in particular smooth across both planes and the focal parabolas. This is how the global matching left open in Sec. 2.2 is satisfied.

3. *The grounded electrode.* $M(\mu_0) = 0$, that is [13, (6.2)]

$$F(\mu_0) = \mathrm{Ce}_{2n}(\alpha_0, q) = 0, \qquad \sinh^2 \alpha_0 = \frac{\mu_0 - b}{b - c} = \tfrac{3}{2}. \tag{28}$$

For each n this has an infinite sequence of positive roots $q_{n0} < q_{n1} < \cdots$, and $\mathrm{Ce}_{2n}(\alpha, q_{nm})$ has exactly m zeros in $0 < \alpha < \alpha_0$.

Thus one separation constant is fixed through the integer n by single-valuedness, and the other through m by the boundary. Neither condition alone determines both. The lowest roots are listed in Table 2.

$2n$	m	q	a	α_3	α_2
0	0	0.7697233298	−0.2792811314	0.3848616649	0.6999030470
2	0	3.0705009820	6.1045410707	1.5352504910	4.5966362496
0	1	4.4890713938	−5.0163744356	2.2445356969	3.2349777848
4	0	6.9838022610	18.4038659161	3.4919011305	11.5847687400
2	1	8.5043910926	8.0667778762	4.2521955463	10.5210855617
0	2	11.5284191405	−16.5266588431	5.7642095702	7.3967544297

Table 2: Lowest roots of Eq. (28) for $b = 3$, $c = 1$, $\mu_0 = 6$, with $a = a_{2n}(q)$ and the separation constants. These values are our own computations. Three methods agree to better than 10^{-12}: direct integration of the separated equations, a 50-digit Fourier-series evaluation with the characteristic value from a continued fraction, and an independent library implementation of the radial Mathieu functions. The first 30 roots also agree to about 10^{-6} with Dirichlet eigenvalues (the allowed values when the function is required to vanish on the boundary) of the ellipse $\alpha < \alpha_0$, computed without Mathieu functions. Arscott notes that roots of this kind were tabulated by Ince for small orders [13, p. 137]; we did not consult those tables.

One checks that the reflection $(x, y, z) \mapsto (y, x, b + c - z)$ maps the confocal family onto itself by $\sigma \mapsto b + c - \sigma$, swapping the μ and ν families, while the unified $k = 0$ equation keeps its form with $(a, q) \mapsto (a, -q)$. The problem with the two paraboloids exchanged is therefore the same as the one treated here, on another such region. This is the geometric content of Arscott's identity $\mathrm{CE}_{2n}(z, q) = (-1)^n \mathrm{Ce}_{2n}(z, -q)$ for his co-Mathieu function CE_{2n} [13, (5.2)].

6.3 An exact single-mode solution

Take the lowest root, $q = q_{00} = 0.7697233298$. Inverting Eq. (25) gives

$$a = -0.2792811314, \qquad \alpha_3 = 0.3848616649, \qquad \alpha_2 = 0.6999030470, \tag{29}$$

and with F from Eq. (27) for $n = 0$,

$$V = V_0 \, \frac{F(\mu)\, F(\nu)\, F(\lambda)}{F(b)\, F(0)\, F(c)}. \tag{30}$$

Each factor solves its own ODE of Sec. 4 with the same α_2, α_3, so V is harmonic in Ω (it satisfies Laplace's equation there). It vanishes on $\mu = \mu_0$ by Eq. (28). On $\nu = 0$ it equals $V_0 F(\mu)F(\lambda)/[F(b)F(c)]$, which is V_0 at the vertex $z = 0$ and falls to zero at the rim. Equation (30) is therefore the exact solution for that prescribed electrode potential. It is the nonzero-constant counterpart of Eq. (15). On the axis $x = y = 0$ two of the three coordinates sit at the endpoints b and c and the third equals z, so there $V/V_0 = F(z)/F(0)$. For example, $V/V_0 = 0.5296034918$, 0.2077175586 and 0.0914804716 at $z = 2$, 4 and 5.

We checked Eq. (30) at 30 digits. The Cartesian Laplacian vanishes to 10^{-30} at points that include the planes $x = 0$ and $y = 0$, and $F(\mu_0)$ vanishes to the same accuracy. Across both planes, in all four charts of Sec. 2.2, V changes quadratically rather than linearly in the transverse coordinate. These checks are in the ancillary file `check_v2_arscott_example.py`. Figure 7 shows the equipotentials.

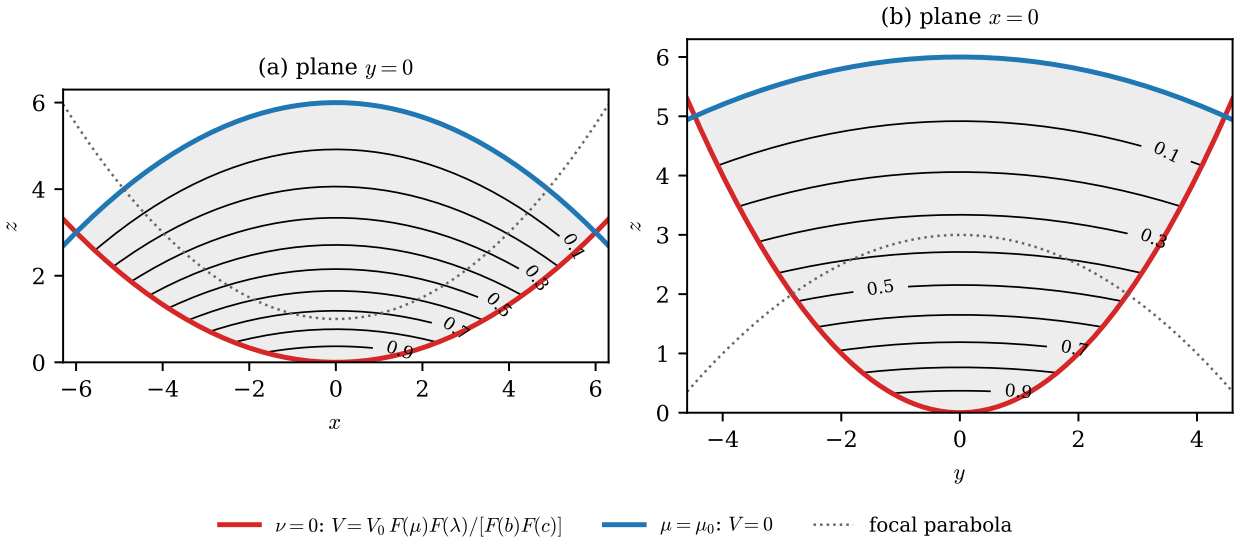


Figure 7: Equipotentials $V/V_0 = 0.1, \ldots, 0.9$ of the single-mode solution, Eq. (30), between the electrode $\nu = 0$ (red), whose potential is V_0 at the vertex and falls to zero at the rim, and the grounded electrode $\mu = 6$ (blue); $b = 3$, $c = 1$. (a) Plane $y = 0$; (b) plane $x = 0$. Dotted curves are the focal parabolas; the field is smooth across them.

6.4 Constant potential on $\nu = 0$: a series

For the constant potential V_0 on $\nu = 0$ no single mode suffices. We superpose

$$V = V_0 \sum_{n,m} C_{nm}\, \frac{F_{nm}(\mu)\, F_{nm}(\nu)\, F_{nm}(\lambda)}{F_{nm}(0)}, \tag{31}$$

where F_{nm} is Eq. (27) at $q = q_{nm}$. On $\nu = 0$ the products $u_{nm} = F_{nm}(\mu)F_{nm}(\lambda)$ are orthogonal with weight $\cosh 2\alpha - \cos 2\beta = 2(\mu - \lambda)/(b - c)$ over $0 < \alpha < \alpha_0$, $-\pi < \beta \le \pi$ (orthogonal here means $\iint u_{nm}\, u_{n'm'}\, (\cosh 2\alpha - \cos 2\beta)\, d\alpha\, d\beta = 0$ for $(n, m) \neq (n', m')$, not a right angle between surfaces) [13, (6.7)–(6.8)]. Hence

$$C_{nm} = \frac{\iint u_{nm}\, (\cosh 2\alpha - \cos 2\beta)\, d\alpha\, d\beta}{\iint u_{nm}^2\, (\cosh 2\alpha - \cos 2\beta)\, d\alpha\, d\beta}, \tag{32}$$

which is Arscott's (6.9)–(6.10). Because $\partial_\alpha^2 u_{nm} + \partial_\beta^2 u_{nm} = -2q_{nm}(\cosh 2\alpha - \cos 2\beta)\, u_{nm}$, the numerator equals $-(\pi/q_{nm})A_0^{(2n)}\, \partial_\alpha \mathrm{Ce}_{2n}(\alpha_0, q_{nm})$. The normalization of F_{nm} cancels from Eq. (31).

With the 118 terms having $q_{nm} \le 240$ (orders $2n \le 36$), $V/V_0 = 0.63415562$ at $(0, 0, 3)$ and 0.20156986 at $(0, 0, 5)$. Both values change by about 10^{-8} when the number of terms is halved. A Cartesian finite-difference solution that uses no Mathieu functions agrees to within 2×10^{-5} after extrapolation to zero grid spacing. The series vanishes on $\mu = \mu_0$ to 10^{-14}, its Laplacian is zero to the accuracy of the finite-difference test ($\sim 10^{-8}$ relative), and it is smooth across both symmetry planes and the focal parabolas.

The series converges slowly near the electrode $\nu = 0$. The reason is that the prescribed potential jumps from V_0 to 0 at the rim, where the two electrodes meet, while every term vanishes on $\mu = \mu_0$. On $\nu = 0$ itself the series is an eigenfunction expansion of a function that does not vanish at the edge of its domain. Like a Fourier sine series for a constant, it converges there only in the mean: the mean-square error tends to zero, but the sum need not approach the boundary value at each point. The relative mean-square misfit falls as roughly $q_{\max}^{-1/4}$ and is still 17% at $q_{\max} = 240$. Inside Ω each term carries the factor $F_{nm}(\nu)/F_{nm}(0)$. In our computations this factor becomes small for large q_{nm} away from $\nu = 0$, so convergence improves quickly with distance from the electrode. Near the rim, where every contour meets, it remains slow. We therefore show the series on the axis rather than as contours (Fig. 8). The axis values are converged except within about one unit of the electrode vertex, where the two truncations shown differ. This is the electrostatic counterpart of the Gibbs phenomenon, the overshoot of a Fourier series at a jump. A Fourier series for a square wave overshoots the jump by about 9% of its height, however many terms are kept, because every finite sum is continuous and must cross the jump smoothly. Here the jump sits at the rim. The boundary data are V_0 on $\nu = 0$ and 0 on $\mu = \mu_0$, but each term, and so each finite sum, is continuous and vanishes on $\mu = \mu_0$. A finite sum must therefore fall from about V_0 to 0 over a short distance near the rim, and it overshoots on the way. Figure 9 shows this just inside the electrode in the plane $y = 0$.

How large is the overshoot? The exact solution cannot exceed V_0 anywhere in Ω, because a harmonic function takes its largest value on the boundary of its region (the maximum principle). Each finite sum is harmonic too, and it is zero on $\mu = \mu_0$, so its largest value is reached on the electrode $\nu = 0$. We therefore found the peak by searching that surface. With $q_{\max} = 240$ (118 terms) it is $V/V_0 = 1.19$, at a straight-line distance 0.68 from the rim. The peak lies between the planes $x = 0$ and $y = 0$; in the plane $y = 0$ of Fig. 9 the bump is slightly lower.

This excess is not a feature of the solution. At any fixed point inside Ω the series converges to the true potential, so there the excess disappears as terms are added. The overshoot survives only by moving closer to the rim, as the Fourier overshoot moves closer to the jump. Our computations show both effects. On the surface $\nu = 0.05$, slightly inside the electrode, the largest value of the sum falls from 1.17 with 15 terms to 1.02 with 466 terms. Meanwhile each doubling of the number of terms cuts the distance from the peak to the rim by about 30%, from 1.95 with 15 terms to 0.34 with 466 terms. The height of the peak changes little: it is 1.22, 1.21, 1.20, 1.19, 1.19 and 1.19 with 15, 30, 59, 118, 234 and 466 terms. Over the last fourfold increase in the number of terms it stays between 1.187 and 1.191. It has nearly leveled off, but our data cannot tell whether it settles to a fixed value, as the Fourier overshoot does, or keeps falling slowly. The analogy is in the cause, not in the number.

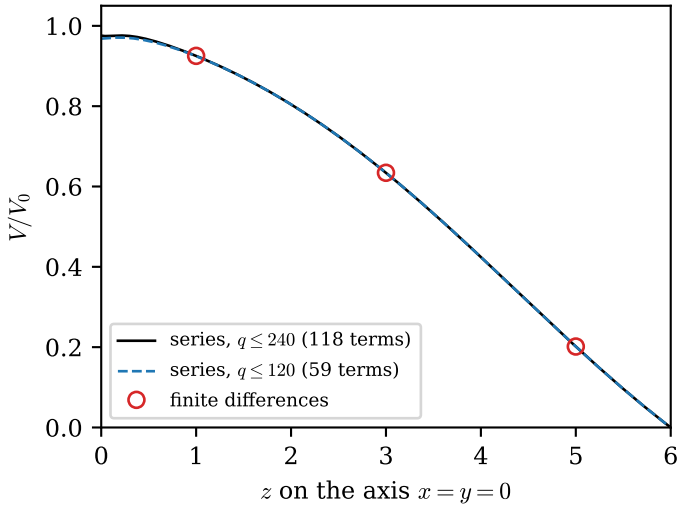


Figure 8: Potential on the axis for constant potential V_0 on $\nu = 0$ and $V = 0$ on $\mu = 6$, from Eq. (31) with 118 terms (solid) and 59 terms (dashed). Circles are a Cartesian finite-difference solution extrapolated to zero spacing. Near $z = 0$ the truncated series has not converged and does not yet reach V_0. This is the slow convergence at the electrode described in the text.

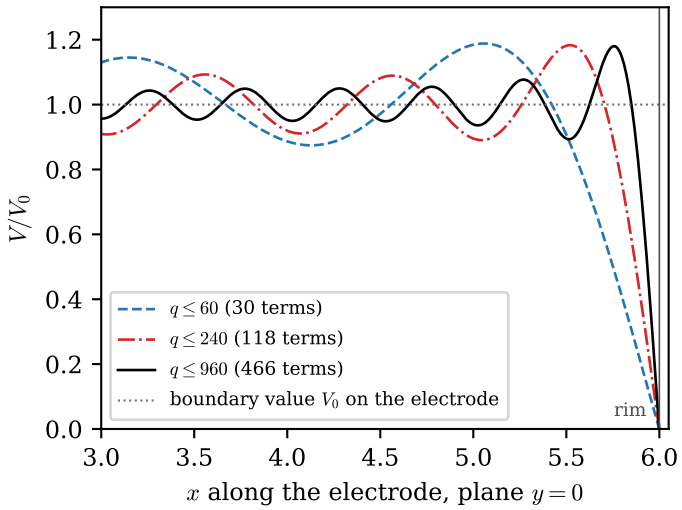


Figure 9: The truncated series, Eq. (31), just inside the electrode (on the surface $\nu = 0.001$) in the plane $y = 0$, from $x = 3$ out to the rim at $x = 6$, with 30, 118 and 466 terms. The dotted line is the boundary value V_0. Every finite sum falls to zero at the rim, because each term vanishes on $\mu = \mu_0$, and it overshoots V_0 just before the fall. As terms are added the bump narrows and moves toward the rim while its height stays near 1.18 in this plane, and the ripples farther from the rim shrink. All curves are our computation.

7 Example: the region outside one paraboloid

This section is included for teaching reasons, not as a new result, as far as the integral-transform method is concerned. It shows how the separated solutions of Secs. 4–6 are used when the region is unbounded in the μ direction, so that the discrete series of Sec. 6 is replaced by an integral. The integral-transform method we follow was given by Darai and Arscott [18] (and in Darai's thesis [19, Ch. 3]) for a mixed boundary-value problem on the degenerate plate $\alpha = 0$ (the potential is prescribed on part of the plane and its normal derivative, zero in their problem, on the rest), which the elasticity literature calls a punch problem: a rigid punch pressed into an elastic half-space. The inversion identity they use is due to McLachlan [20, §§10.50–10.51]. The same construction applies to the Dirichlet problem outside a non-degenerate electrode $\mu = \mu_0$, the only change being that the decaying radial factor is the ratio $\mathrm{Fek}_{2n}(\alpha, -p)/\mathrm{Fek}_{2n}(\alpha_0, -p)$ rather than $\mathrm{Fek}_{2n}(\alpha, -p)/\mathrm{Fek}_{2n}(0, -p)$. We state the problem in our coordinates, record the condition at infinity with a uniqueness check, and give a fully checked numerical example. At the end we derive the far-field decay of the potential. We have not found this asymptotic law stated in the literature we checked: Lebedev, Skalskaya and Uflyand give the exact Hankel-transform solution for a paraboloid of revolution, but not its far field [24, pp. 231–233]; Lebedev's textbook treats these coordinates only as an exercise on separation [23, Problem 8, p. 299]; Darai and Arscott impose decay at infinity without deriving a rate; and Arscott's Helmholtz paper [14] concerns $k^2 < 0$ inside a paraboloid, imposes decay through the choice of solutions, and does not treat Laplace's equation. As far as that search went, the decay law is our own contribution.

7.1 The problem, and why a condition at infinity is needed

Keep $b = 3$, $c = 1$ and the electrode $\mu = \mu_0 = 6$ of Secs. 5–6. The region is now the exterior of that downward paraboloid,

$$\Omega = \{\mu > \mu_0\}, \tag{33}$$

that is, $z > 6 - x^2/12 - y^2/20$, using the extension $\nu < 0$ of Sec. 2.2. In Arscott's angles (26), $\alpha > \alpha_0$ with $\sinh^2 \alpha_0 = (\mu_0 - b)/(b - c) = 3/2$, while β and γ run over their full ranges. The potential V is prescribed on $\mu = \mu_0$, say $V = f$, and we seek V harmonic in Ω. We treat data even in x and in y; the other parity classes are analogous.

Without a condition at infinity the solution is not unique. One may add any multiple of $G(\mu) - G(\mu_0)$, with G the logarithmic solution (15) of Sec. 5: the difference is harmonic, vanishes on $\mu = \mu_0$, and grows like $\ln \mu$. A condition at infinity is therefore part of the problem. If the data f tend to 0 at infinity on the electrode and we require $V \to 0$ at infinity in Ω, uniqueness follows from the maximum principle on large balls. In three dimensions a solution with $V \to 0$ exists for any continuous data that tend to 0 at infinity on the electrode, because the point at infinity is a regular boundary point of every unbounded open set [21, Thm. 6.7.1]: a regular boundary point is one at which the Dirichlet solution takes the prescribed continuous boundary value. If we require only that V be bounded, uniqueness holds when the complement (everything not in Ω, here the solid paraboloid) is *thick at infinity*, which Armitage and Gardiner call non-thin at infinity [21, Sec. 7.6]: the complement is large enough at large distance, in the capacity test below (capacity meaning the charge a conductor holds at unit potential, in units where a point charge q has potential q/r). In that case the point at infinity is *negligible for* Ω [21, Thm. 7.6.5(ii)] in their technical sense [21, Def. 6.5.1]: the Dirichlet solution with value 1 at infinity and 0 on the electrode is identically zero, so the point at infinity does not affect the solution. This does not mean "small." Equivalently, there is a positive superharmonic function on Ω (one whose value at each point is at least its average over small spheres about that point; for a smooth function this is $\nabla^2 s \le 0$) that

tends to $+\infty$ at infinity [21, Thm. 6.5.2], and a bounded harmonic function in Ω is therefore fixed by its values on the finite boundary.

The test is Wiener's criterion [21, Thm. 7.7.2]; see also Abdulla and Brazke [22] for a much more general treatment.[9]

Cut the complement into annular pieces at radii 2^k, compute the electrostatic capacity of each piece, and ask whether the series of those capacities, each divided by 2^k, diverges. If it does, the complement is thick and the bounded Dirichlet problem has exactly one solution. For a paraboloid, a piece at distance R has length of order R and radius of order $\sqrt{R}$; its capacity is of order $R/\ln R$, so the series behaves like $\sum 1/k$ and diverges. A paraboloid is therefore thick at infinity, and a bounded solution is unique. In particular, constant data V_0 give the constant solution $V \equiv V_0$ in the bounded class.

7.2 From a discrete series to an integral

In the bounded lens (24) of Sec. 6, μ runs over a finite interval and the condition $M(\mu_0) = 0$ selects a discrete sequence of values of q. Here μ runs over the half-line $\mu > \mu_0$. Requiring the μ-factor to decay as $\mu \to \infty$ does not force q onto a discrete set: every $p > 0$ is allowed, together with the Mathieu characteristic value $a = a_{2n}(p)$. A general solution is a superposition, now an integral over p, or equivalently over the wavenumber $k = 2\sqrt{p}$. This is the same distinction as between a Fourier series on a finite interval and a Fourier integral on the line. One says that the problem has a *continuous spectrum*: the allowed values of the separation constant form a continuum, and the expansion is an integral rather than a sum. (The angular order n is still discrete, by 2π-periodicity in β.)

The sign of q is fixed by decay in γ. For $q > 0$ the even ν-factor grows; $q = 0$ leaves only the constant (the logarithmic solution of Sec. 5 is excluded by the condition at infinity). The surviving family is $q = -p$ with $p > 0$, so $\alpha_3 = -p/(b-c)$ and $\alpha_2 = [a_{2n}(p) - 2p(b+c)/(b-c)]/4$. In Arscott's angles the even–even modes are

$$\mathrm{ce}_{2n}(\eta, p)\,\mathrm{Ce}_{2n}(\gamma, p)\,\frac{\mathrm{Fek}_{2n}(\alpha, -p)}{\mathrm{Fek}_{2n}(\alpha_0, -p)}, \qquad \eta = \tfrac{1}{2}\pi - \beta. \tag{34}$$

Here $\mathrm{Ce}_{2n}(\gamma, p)$ is oscillatory in γ and decays like $|\nu|^{-1/4}$. The μ-factor is the modified Mathieu function of the third kind, Fek_{2n}, which is the solution of the radial Mathieu equation that decays as $\alpha \to \infty$ (the analogue of the modified Bessel function K_ν, as opposed to I_ν, which grows). Its leading decay is $\exp\!\big(-2\sqrt{p\mu/(b-c)}\big)$. The paper's entire function F of Eq. (27) grows in α and is not the right radial factor here.

7.3 The electrode as a plane, and the integral transform

The key simplification, already used by Darai and Arscott on the plate $\alpha = 0$, is visible on a non-degenerate electrode as well. On $\mu = \mu_0$ set

$$X = \frac{x}{2\sqrt{(b-c)(\mu_0 - b)}}, \qquad Y = \frac{y}{2\sqrt{(b-c)(\mu_0 - c)}}. \tag{35}$$

For $b = 3$, $c = 1$, $\mu_0 = 6$ the denominators are $2\sqrt{6}$ and $2\sqrt{10}$. Then $X = \cosh\gamma\cos\eta$ and $Y = \sinh\gamma\sin\eta$: the angles (γ, η) are ordinary elliptic coordinates in the (X, Y) plane. The

[9] Armitage and Gardiner state Wiener's criterion at a finite point for the inverted set. Inversion in a sphere turns it into the dyadic series below (pieces at radii 2^k, each twice the previous), with constants that do not affect divergence. We have written out this step, and the capacity estimate for the paraboloid, ourselves; neither is quoted from the book.

coefficients of the line element (6) form the metric tensor of the coordinate system, as in Sec. 3. Restricted to $\mu = \mu_0$ they imply

$$dX\,dY = \tfrac{1}{2}(\cosh 2\gamma + \cos 2\beta)\,d\gamma\,d\eta, \tag{36}$$

so the weight that makes the Mathieu products orthogonal on the electrode (the weight w for which $\int f\,g\,w = 0$ when f and g are two different products) is, up to a constant, the ordinary area element $dX\,dY$. Orthogonality of the Mathieu products on the electrode is therefore ordinary orthogonality of functions of (X, Y) in the plane, $\int f\,g\,dX\,dY$, and finding the allowed separation constants becomes the planar Helmholtz problem with wavenumber $k = 2\sqrt{p}$. The expansion of the data is just the two-dimensional Fourier transform of f as a function of (X, Y), followed by a decomposition of each plane wave into Mathieu angular factors. McLachlan's identity [20, 10.50 (13)] supplies that decomposition; it is the inversion identity used in [18]. The only specifically paraboloidal ingredient is the decaying ratio of Fek functions in (34), which continues each component off the electrode.

For data even in x and y, writing $\hat{F}(k, \theta)$ for the Fourier transform of $f(X, Y)$, $\hat{C}_{2n}(\gamma, p) = \mathrm{Ce}_{2n}(\gamma, p)/\mathrm{ce}_{2n}(0, p)$ and $R_{2n}(\alpha, p)$ for the Fek ratio in (34), the solution is

$$V = \frac{1}{4\pi^2}\int_0^\infty k\,dk \sum_{n=0}^{\infty} \frac{2A_0^{(2n)}\,g_n(k)}{\mathrm{ce}_{2n}(\pi/2, p)}\,\mathrm{ce}_{2n}(\eta, p)\,\hat{C}_{2n}(\gamma, p)\,R_{2n}(\alpha, p), \tag{37}$$

with $p = k^2/4$ and $g_n(k) = \int_0^{2\pi} \hat{F}(k, \theta)\,\mathrm{ce}_{2n}(\theta, p)\,d\theta$. On $\alpha = \alpha_0$ the ratio R is 1 and (37) reduces to Fourier inversion, so the boundary data are recovered by construction.

7.4 A worked example

Take the Gaussian spot $f = \exp\bigl[-(X^2 + Y^2)\bigr]$, circularly symmetric in (X, Y) (its level curves are ellipses in x, y), on $\mu = \mu_0$, or $\exp\bigl[-(x/2\sqrt{6})^2 - (y/2\sqrt{10})^2\bigr]$ in Cartesian coordinates. It is even, nonconstant, and tends to 0 at infinity on the electrode. For this data the angular integrals in (37) can be done in closed form, and

$$V = \int_0^\infty k\,e^{-k^2/4} \sum_{n=0}^{\infty} \frac{\bigl(A_0^{(2n)}\bigr)^2}{\mathrm{ce}_{2n}(\pi/2, p)}\,\mathrm{ce}_{2n}(\eta, p)\,\hat{C}_{2n}(\gamma, p)\,R_{2n}(\alpha, p)\,dk. \tag{38}$$

Selected values are given in Table 3. Figure 10 shows the equipotentials in the two symmetry planes.

(x, y, z)	V
$(0, 0, 6.5)$	0.8352507804
$(0, 0, 8)$	0.5353514075
$(0, 0, 15)$	0.1584493245
$(3, 0, 6)$	0.6076381908
$(10, 0, 0)$	0.0502742017
$(15, 0, -5)$	0.0154782800

Table 3: Potential of the Gaussian example, Eq. (38), at six points in Ω. These are our computations. A change of the k-quadrature (the numerical integration over k; its nodes are the sample points of the integration rule) from $(40, 80, 160)$ nodes with $k_{\max} = 12$ to twice as many nodes with $k_{\max} = 14$ changes every entry by at most 5.5×10^{-13}.

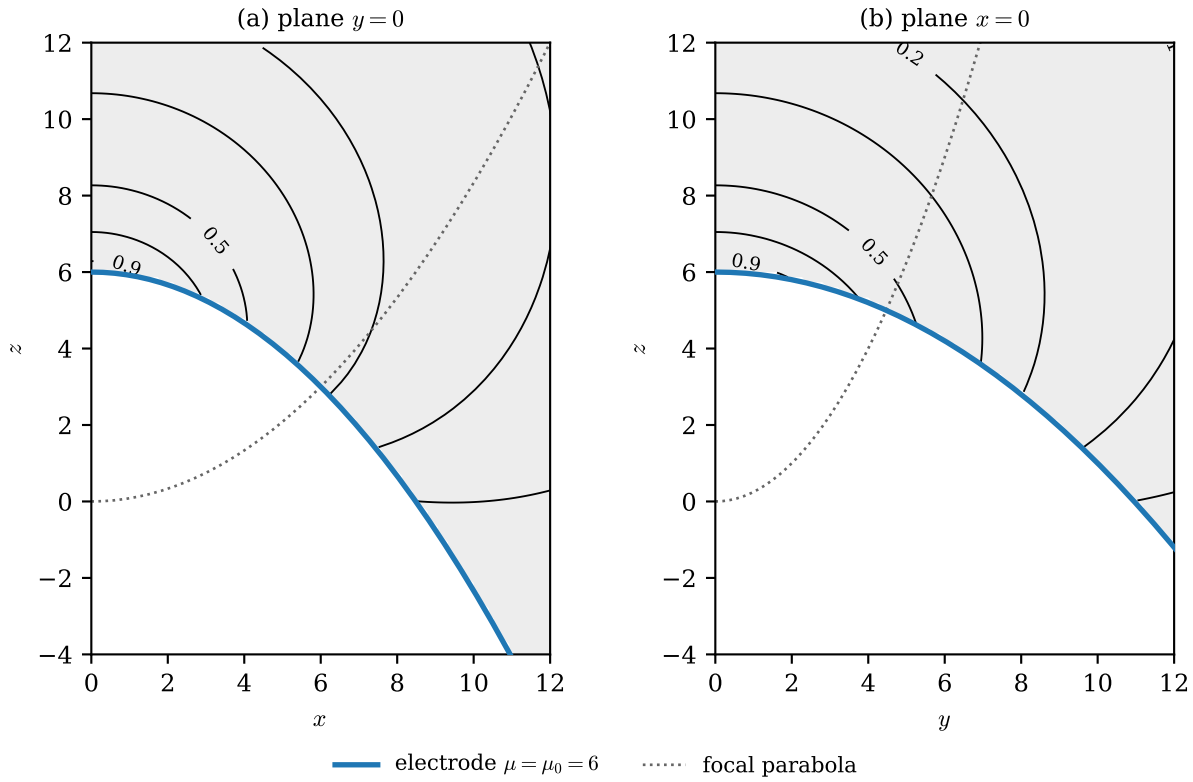


Figure 10: Equipotentials $V = 0.05, 0.1, 0.2, 0.3, 0.5, 0.7, 0.9$ of the Gaussian example, Eq. (38), in the exterior region $\Omega = \{\mu > 6\}$ (shaded); $b = 3$, $c = 1$. The electrode $\mu = 6$, on which $V = \exp[-(X^2 + Y^2)]$, is the bold curve. (a) Plane $y = 0$; (b) plane $x = 0$. Dotted curves are the focal parabolas. All curves are our computation.

We checked (38) in four independent ways, all in Ω. On the electrode, $\max|V - f|$ is 1.9×10^{-13} at 30 random points with $|X|, |Y| \le 3$, and 7.8×10^{-14} at 30 farther points with $|X|, |Y| \le 8$. A Cartesian finite-difference Laplacian at seven interior points (including points on $x = 0$ and $y = 0$, one with $\nu < 0$, and one near a focal parabola) is at most 8.3×10^{-11}. An independent numerical solution, using no Mathieu functions and no separation, was obtained by the method of fundamental solutions: one places fictitious point charges, sources of the Coulomb potential $1/|\mathbf{r} - \mathbf{r}_j|$, inside the solid paraboloid, and chooses their strengths so that the potential matches f at chosen points on $\mu = \mu_0$ (the collocation points). Every such sum is exactly harmonic and tends to 0 at infinity. The greatest difference from (38) at 15 test points falls from 6.3×10^{-4} at collocation radius 20 to 1.7×10^{-5} at radius 160 with a refined point set; at $(0, 0, 8)$ the values are 0.53534772 and 0.53535141, respectively, and the gap shrinks steadily as the collocation patch is enlarged. Finally, as $b \to c$ with the same physical data, (37) reduces to the classical Hankel-transform solution for a paraboloid of revolution [24, pp. 231–233], built from the factors $J_0(\lambda v)\, K_0(\lambda u)/K_0(\lambda u_0)$. At $b - c = 0.004$ the greatest difference from that formula, at six test points, is 5.1×10^{-5}; Richardson extrapolation to $b = c$ (combining results at different values of $b - c$ to estimate the limit $b - c = 0$) agrees to 1.2×10^{-7}.

7.5 Far-field decay

We now derive how V falls off at large distance. As already noted, we have not found this asymptotic law stated in the literature we checked.

Start with the paraboloid of revolution, $b = c$, for which the exact solution is the Hankel integral just recalled. The natural coordinates are then the rotational parabolic pair (u, v), with $u \geq 0$, $v \geq 0$, related to cylindrical (ρ, z) by $z - c = u^2 - v^2$ and $\rho = 2uv$. Lebedev sets the separation of Laplace's equation in these coordinates as an exercise [23, Problem 8, p. 299]: his formulas for Cartesian position are $x = c\alpha\beta\cos\varphi$, $y = c\alpha\beta\sin\varphi$, $z = \frac{1}{2}c(\alpha^2 - \beta^2)$, which agree with ours when his length parameter is $c = 2$ and $(\alpha, \beta) = (u, v)$, his z being our $z - c$. The combination $R = u^2 + v^2$ is the distance from the field point to the focus $(0, 0, c)$. The electrode $\mu = \mu_0$ is the surface $u = u_0$, with $u_0 = \sqrt{\mu_0 - c}$, and the exterior Ω is $u > u_0$. Along a straight ray from the focus, at a fixed polar angle θ from the positive z-axis, the ratio $\kappa = v/u$ is constant and equals $\tan(\theta/2)$. Figure 11 is a sketch of this geometry.

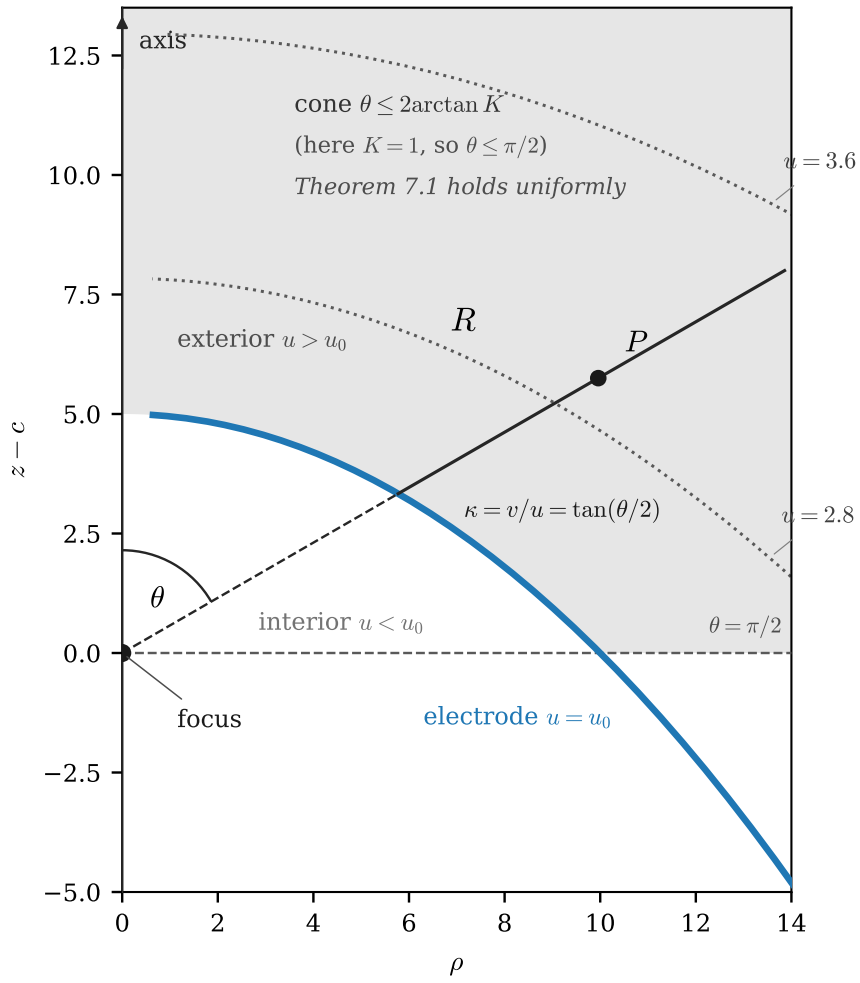


Figure 11: Meridian plane through the axis, for the paraboloid of revolution $b = c$. The origin is at the focus, so the vertical axis is $z - c$. The bold curve is the electrode $u = u_0$ (drawn for $u_0 = \sqrt{5}$, as in the Gaussian example below); the exterior Ω is $u > u_0$, on the side away from the focus. A sample field point P lies on a ray from the focus at polar angle θ, at distance $R = u^2 + v^2$; along that ray the ratio $\kappa = v/u = \tan(\theta/2)$ is constant. Dotted curves are surfaces of constant $u > u_0$, which recede to infinity as u grows. The shaded region is the cone $\theta \le 2\arctan K$ in the exterior, drawn for $K = 1$ so that $\theta \le \pi/2$. Theorem 7.1 holds uniformly (the size of the error bound does not depend on the direction inside the cone) throughout any such closed cone (including its edge); it is not claimed as $\theta \to \pi$, where the rays graze the far sheets of the electrode.

For axisymmetric data $f(v)$ on the electrode, decaying rapidly at large v, the Hankel transform of the data is the integral $\tilde{a}(\lambda) = \int_0^\infty f(v)\, J_0(\lambda v)\, v\, dv$, a number for each wavenumber $\lambda > 0$. In particular $\tilde{a}(0) = \int_0^\infty f(v)\, v\, dv$ is a single constant determined by f. (For the Gaussian $f = e^{-v^2}$ one has $\tilde{a}(0) = 1/2$.) The inversion, which recovers f from $\tilde{a}$, is Hankel's integral theorem [23, Eq. (5.14.11), p. 130]: on the electrode, $f(v) = \int_0^\infty \lambda\, \tilde{a}(\lambda)\, J_0(\lambda v)\, d\lambda$. The potential is

$$V(u, v) = \int_0^\infty \lambda\, \tilde{a}(\lambda)\, J_0(\lambda v)\, \frac{K_0(\lambda u)}{K_0(\lambda u_0)}\, d\lambda. \tag{39}$$

With this notation the far-field law is as follows.

Theorem 7.1 (Far-field decay, paraboloid of revolution).

Let the electrode data $f(v)$ be axisymmetric with $\int_0^\infty (v+v^3)\,|f(v)|\,dv < \infty$; then $\tilde{a}(\lambda) = \tilde{a}(0) + O(\lambda^2)$. Fix $K \geq 0$. Then, as $u \to \infty$, uniformly for $0 \leq \kappa \leq K$ (the closed cone $\theta \leq 2\arctan K < \pi$ about the focus, including its edge; uniformly: the size of the error bound does not depend on the direction κ inside the cone),

$$V = \frac{\tilde{a}(0)}{R\ln\bigl(R/(uu_0)\bigr)} + O\biggl(\frac{1}{R(\ln u)^3}\biggr). \tag{40}$$

In words: the potential falls off like $1/(R\ln R)$, slightly faster than a point charge. The logarithm may equally be written $\ln(u/u_0)+\ln(1+\kappa^2)$, and the leading constant $C = \tilde{a}(0)$ is independent of direction.

Proof (sketch). The proof is a large-u expansion of (39); the algebraic steps were checked with `mpmath`. Substitute $t = \lambda u$, so $d\lambda = dt/u$ and $\lambda u = t$. Then

$$V = u^{-2}\int_0^\infty t\,\tilde{a}(t/u)\,J_0(\kappa t)\,\frac{K_0(t)}{K_0(tu_0/u)}\,dt. \tag{41}$$

At large u, two simplifications occur. First, $\tilde{a}(t/u) \to \tilde{a}(0)$ on any fixed range of t, and the difference $\tilde{a}(t/u) - \tilde{a}(0) = O(t^2/u^2)$ produces, after integration against $tK_0(t)$, an error smaller than the remainder we keep. Second, $K_0(t)$ decays exponentially for large t, so only t of order 1 contributes: the corresponding wavenumbers are $\lambda = t/u = O(1/u)$, which is why only the small-λ behaviour of $\tilde{a}$ and of $K_0(\lambda u_0)$ can matter. On that range tu_0/u is small, and the small-argument expansion $K_0(z) = -\ln(z/2) - \gamma + O(z^2\ln z)$ applies, with γ the Euler constant. If $K_0(\lambda u_0)$ were replaced by a constant, the identity[10]

$$\int_0^\infty \lambda\,J_0(\lambda v)\,K_0(\lambda u)\,d\lambda = \frac{1}{u^2+v^2}, \tag{42}$$

or, after the same substitution, $\int_0^\infty t\,J_0(\kappa t)\,K_0(t)\,dt = 1/(1+\kappa^2)$, would give $V = \tilde{a}(0)/R$ exactly. It is not a constant: it is a logarithm of a small quantity, and (41) instead produces $\tilde{a}(0)$ divided by R times that logarithm. Writing $K_0(tu_0/u) = \ln(u/u_0) + \beta - \delta(t) + \cdots$ and choosing the additive constant β so that the first correction $\int t\,J_0(\kappa t)\,K_0(t)\,\delta(t)\,dt$ vanishes, one finds $\beta = \ln(1+\kappa^2)$. The combination is $\ln(u/u_0)+\ln(1+\kappa^2) = \ln\bigl(R/(uu_0)\bigr)$, which is (40). The next term in the expansion of $1/K_0$ is of order $1/(\ln u)^3$ after this choice of β, and multiplying by u^{-2} gives the stated remainder. The evaluation of β, and of the next coefficient $\pi^2/12$ on the axis, is a short calculation with the Mellin transform of $J_0(\kappa t)K_0(t)$ (the Mellin transform of a function g is $\int_0^\infty t^{s-1}g(t)\,dt$; here its value at $s=2$ and its s-derivative there give the needed integrals exactly). Appendix C gives the full proof, with explicit bounds on every discarded piece: the change from $\tilde{a}(t/u)$ to $\tilde{a}(0)$, the large-t tail, and the remainder in the expansion of $1/K_0$. □

Table 4 checks (40) against a high-precision quadrature of the exact integral (39), for the Gaussian $\tilde{a}(\lambda) = e^{-\lambda^2/4}/2$ with $u_0 = \sqrt{5}$. The reported ratio is $VR\ln\bigl(R/(uu_0)\bigr)/\tilde{a}(0)$, which the theorem says tends to 1. On the axis, $\kappa = 0$ and the first correction vanishes, so the ratio should approach 1 like $1 + \pi^2/(12L^2)$ with $L = \ln(u/u_0)$; that two-term prediction is listed beside the

[10] This is the limiting case $y \to 0$ of Lebedev [23, Eq. (5.15.6), p. 134], with $\mu = \nu = 0$, $a = u$ and $b = v$, using $K_{-1} = K_1$ and $K_1(z) \sim 1/z$ as $z \to 0$.

computed ratio. At $\theta = \pi/2$, the factor $\ln(1+\kappa^2) = \ln 2$ is essential: omitting it leaves the ratio 13% low even at $R = 40960$. Figure 12 shows the same comparison: $RV/\tilde{a}(0)$ falls slowly, like $1/\ln(R/(uu_0))$, whereas for a point charge RV would be constant.

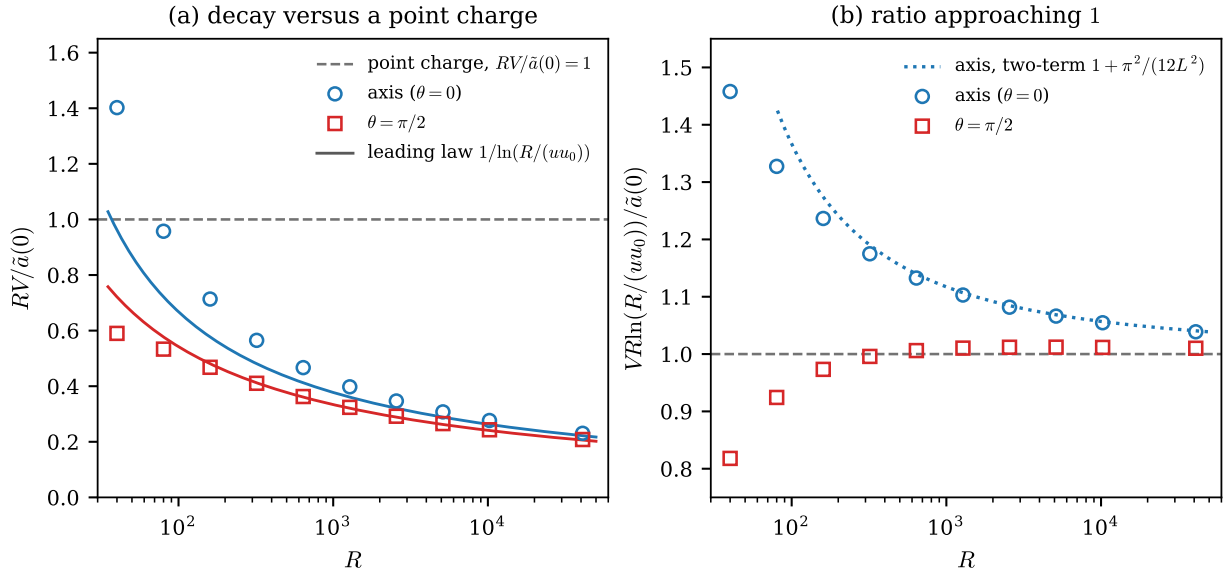


Figure 12: The Gaussian example of Table 4, $u_0 = \sqrt{5}$, $\tilde{a}(0) = 1/2$. (a) The quantity $RV/\tilde{a}(0)$, on the axis and at $\theta = \pi/2$, from a high-precision quadrature of (39). The solid curves are the leading law $1/\ln(R/(uu_0))$ of Theorem 7.1; the dashed horizontal line is a point-charge decay $V \propto 1/R$, for which RV is constant. The computed potential falls slightly faster than a point charge, because of the slowly growing logarithm. (b) The ratio $VR\ln(R/(uu_0))/\tilde{a}(0)$ from the same computation, which the theorem says tends to 1. The dotted curve is the two-term axis prediction $1+\pi^2/(12L^2)$, with $L = \ln(u/u_0)$. All points are our computations.

R	axis, ratio	axis, $1+\pi^2/(12L^2)$	$\theta = \pi/2$, ratio
160	1.2365	1.2739	0.9733
640	1.1326	1.1397	1.0061
1280	1.1030	1.1070	1.0104
10240	1.0546	1.0566	1.0116
40960	1.0389	1.0405	1.0101

Table 4: Check of Eq. (40) for the Gaussian $\tilde{a}(0) = 1/2$, $u_0 = \sqrt{5}$. The ratio is $VR\ln(R/(uu_0))/\tilde{a}(0)$, computed from a high-precision quadrature of (39). On the axis, $L = \ln(u/u_0)$, and the third column is the two-term prediction of that ratio. All entries are our computations.

The elliptic case $b > c$ is not covered by the theorem. Write $\hat{F}(0) = \int f\,dX\,dY$ for the two-dimensional Fourier transform of the data at zero wavenumber, $u_* = \cosh\alpha$, $\ell_0 = e^{\alpha_0}/2$, and $R_* = u_*^2 + \rho_{\text{aux}}^2 = (\mu + b - \nu - \lambda)/(b - c)$, where $\rho_{\text{aux}}^2 = X^2 + Y^2$ is computed from the auxiliary

coordinates (γ, η) alone.

Asymptotic argument (elliptic case, not a proof).

At large distance only small wavenumbers k contribute, because of the decaying Fek factor, and only the $n = 0$ Mathieu term survives for rapidly decaying data; for small k this term has no angular dependence in the auxiliary plane. In this regime the Fek ratio tends to a ratio of modified Bessel functions K_0, with argument $ke^{\alpha}/2$ [20, 11.12], and the transverse factor tends to $J_0(k\rho_{\mathrm{aux}})$ in the auxiliary plane (35). The integral then has the same form as (39), and the same expansion gives

$$V \sim \frac{\hat{F}(0)/(2\pi)}{R_* \ln\bigl(R_*/(u_*\ell_0)\bigr)}. \tag{43}$$

As $b \to c$ one has $u_*\sqrt{b-c} \to u$ and $\ell_0\sqrt{b-c} \to u_0$, and (43) reduces to Theorem 7.1. A rigorous proof would need a uniform Mathieu-to-Bessel limit in the joint regime $k \to 0$, $\alpha \to \infty$ with ke^{α} of order one; that justification is left open.

In the Gaussian example, the $n = 0$ term already reproduces the full potential to four digits at distance 320 and beyond. For $b = 3$, $c = 1$, $\mu_0 = 6$, one has $\hat{F}(0) = \pi$, so the prefactor in (43) is $1/2$. The ratio $VR_* \ln\bigl(R_*/(u_*\ell_0)\bigr)/(\hat{F}(0)/(2\pi))$ at distance 1280 is 1.094 on the axis, against the two-term expectation $1 + \pi^2/(12L^2) = 1.098$, and 1.014, 1.011 along the Cartesian x and y rays. An earlier test that omitted $\ln(1 + \kappa^2)$ gave 0.76 on those rays at the same distance, still drifting; the missing logarithm accounts for the gap.

Two other points are left open. The odd parity classes, involving the se functions, are expected to go in the same way and are not written out here. The uniqueness argument for the bounded class uses Wiener's criterion as in Armitage and Gardiner (Thms. 6.5.2, 7.6.5 and 7.7.2); the capacity estimate that shows a paraboloid is thick at infinity is our check of that criterion, not a statement quoted from the source.

8 Conclusion

The practical lesson is the same as in cylindrical and spherical coordinates: choose surfaces that fit the boundaries before solving the field equation. For confocal paraboloidal boundaries, Moon and Spencer's (μ, ν, λ) system provides that fit. Its three families are mutually orthogonal, and its Laplacian separates into three ODEs with two shared constants, α_2, α_3.

The formulas for Cartesian position determine the scale factors and hence the vector operators. They also fix the real Laplacian independently of the confirmed misprinted prefactor on p. 45. The separated equations agree with Table 1.11, including the general Helmholtz case with $\kappa^2 = k^2$. At symmetry planes, the local square-root variable is essential: smoothness and reflection parity must be imposed in that variable, not by setting an original-coordinate derivative to zero.

The electrode example shows the simplest use of separation. With $k = \alpha_2 = \alpha_3 = 0$, the potential depends on μ alone and follows from one integration. The field is normal to the electrodes. For $V_2 > V_1$, the charge is negative on the lower-μ electrode and positive on the higher-μ electrode; its magnitude is greatest at each vertex. These are local field and charge results. A total capacitance requires a specified truncation, and uniqueness in an unbounded region requires a condition at infinity.

The second example shows how the two constants interact. With $\alpha_2, \alpha_3 \neq 0$ the three separated equations become Mathieu equations with one shared pair (a, q). Single-valuedness makes a a

Mathieu characteristic value, and the grounded paraboloid then fixes q. One entire function serves as all three factors, which is why the product is smooth across the symmetry planes and the focal parabolas. A single mode gives an exact closed solution for a potential that varies over the electrode. A constant potential on the electrode needs a series, which converges slowly near the rim where the two electrodes meet.

A third example treats the region outside one paraboloid. The integral-transform method is that of Darai and Arscott, included here for teaching; for the paraboloid of revolution we derive the far-field decay of the potential, and we give an asymptotic argument, with numerical evidence, that the same law holds in the elliptic case.

The appendices explain the structure behind the calculation. Appendix A shows how determinant identities cancel the two shared separation constants and retain the Helmholtz term. Appendix B locates the same system in Eisenhart's Euclidean classification as Type IV_2 and supplies the notation map. Appendix C gives the full proof of the far-field law for the paraboloid of revolution.

Smoothness alone fixes only one of the two separation constants, through an integer index. The other becomes discrete only when a boundary such as $\mu = \mu_0$ is imposed. Section 6 solves one such two-parameter problem, following Arscott [13]; general boundary shapes and the Helmholtz case are not treated here (for $k^2 < 0$ inside a paraboloid, see Arscott [14]). The general Stäckel conditions have been compared with Moon and Spencer pp. 5–7 and Morse and Feshbach pp. 655–656; the handbook's p. 45 misprint is confirmed in the copies consulted for this note, including the corrected third printing (Springer, 1988). These limits are separate from the symbolic checks of the formulas used here. A reader can use the worked examples now, while treating those broader questions as further work.

A Introduction to Stäckel separability

Why do these coordinates separate when arbitrary curved coordinates usually do not? Moon and Spencer's Stäckel matrix makes the answer visible. It is a table of functions whose rows belong to the individual coordinates. Its determinant and cofactors recover the metric tensor. The same cofactors cancel the separation constants when the three ODEs are recombined into the original PDE.

This appendix is a sufficient-condition calculation for the system used here, not a proof of the full classification of separable systems. Appendix B gives the historical setting. We keep Moon and Spencer's printed column signs because changing those signs changes the convention for the separation constants.

A.1 Matrix, cofactors, and metric tensor

For a moment use generic coordinate names u^1, u^2, u^3. The superscript labels a coordinate; it is not a power. In an orthogonal system the squared line element is $ds^2 = \sum_i g_{ii}(du^i)^2$, $g_{ii} = h_i^2$, and $g^{1/2} = h_1 h_2 h_3$. Here g is the determinant of the metric tensor g_{ij}, and the inverse diagonal element is $g^{ii} = 1/g_{ii}$. Indices i, j, k below run from 1 to 3; sums are written explicitly. A *Stäckel matrix* has entries depending only on the coordinate of their own row [1, pp. 5–6, (1.23)–(1.24)] [2, pp. 655–656],

$$\mathsf{S} = [S_{ij}(u^i)]_{i,j=1}^{3}, \qquad S = \det \mathsf{S} \neq 0. \tag{44}$$

The determinant S must be nonzero so the matrix can be inverted. A *cofactor* is the signed determinant of the smaller matrix obtained by deleting one row and one column. In particular,

$M_{i1} = (-1)^{i+1} \det \mathsf{S}(i \mid 1)$ deletes row i and column 1. Since the deleted row was the only row containing u^i, this cofactor is independent of u^i. Write M_{ik} for the analogous cofactor of column k. The standard determinant identity gives

$$\sum_{i=1}^{3} S_{ij}(u^i) M_{ik} = \delta_{jk} S. \tag{45}$$

Here δ_{jk} is 1 if $j = k$ and 0 otherwise. For the first-column cofactors the identity reads

$$\sum_i S_{i1} M_{i1} = S, \qquad \sum_i S_{i2} M_{i1} = 0, \qquad \sum_i S_{i3} M_{i1} = 0. \tag{46}$$

The key step is to connect this algebraic table to geometry. Morse and Feshbach identify the first-column cofactors as $M_i = \partial S / \partial \Phi_{i1} = S/h_i^2$ [2, p. 655]; their Φ_{ij} and M_i are our S_{ij} and M_{i1}. Moon and Spencer give the same relation [1, p. 6, (1.25)]. Willatzen and Lew Yan Voon [8, Table 2.1, p. 18] compare these notations. Thus the condition on the metric tensor in this convention is

$$g_{ii} = \frac{S}{M_{i1}}, \qquad \text{or} \qquad g^{ii} = \frac{M_{i1}}{S}. \tag{47}$$

We work where S and M_{i1} are positive, so that $g_{ii} > 0$; in general, the positive square root must be chosen when extracting $g^{1/2}$.

Moon and Spencer state that this relation for the metric tensor, together with $g^{1/2}/S = f_1(u^1) f_2(u^2) f_3(u^3)$, gives the necessary and sufficient conditions for *simple separation* of the scalar Helmholtz equation [1, p. 6, (1.25)]. Here simple separation means an ordinary product, without a coordinate-dependent prefactor. The explicit calculation below verifies the conditions for our system; it does not reproduce the general necessity proof.

For Laplace's equation they give the conditions separately [1, p. 7, (1.27)]:

$$\frac{g_{ii}}{g_{jj}} = \frac{M_{j1}}{M_{i1}}, \qquad \frac{g^{1/2}}{g_{ii}} = f_1 f_2 f_3 M_{i1}. \tag{48}$$

Both follow here from the stronger Helmholtz normalization. The Laplace statement should not be silently replaced by a claim that its first Stäckel column must have the same normalization as the nonzero-κ problem: when $\alpha_1 = 0$, that column does not enter the separated ODEs.

What to notice. The matrix is not a rotation of the coordinate axes. It packages the scale factors in a form whose determinant identities can cancel unwanted coordinate dependence.

A.2 Why Laplace and Helmholtz separate

The condition on the metric tensor is only part of the calculation. We also need the volume factor to separate appropriately. Let $f_i(u^i)$ be positive functions of one coordinate. For ordinary product separation, Moon and Spencer [1, p. 6, (1.25)] give $h_i^2 = S/M_i$ and $g^{1/2} = S f_1 f_2 f_3$. Combining the two conditions gives $g^{1/2}/h_i^2 = M_i \prod_j f_j$, so that the factor independent of u^i is $M_i \prod_{j \neq i} f_j$, as Morse and Feshbach also state [2, p. 655]. This is Eq. (49) with $R = u_{\mathrm{MF}} = 1$.

Morse and Feshbach [2, p. 665] use the more general ansatz $\psi = X_1 X_2 X_3 / R$ and factor $h_1 h_2 h_3 / h_i^2 = g_i f_i R^2$, where g_i is independent of the coordinate of row i. Their volume relation is

$$g^{1/2} = R^2 S f_1 f_2 f_3 \, u_{\mathrm{MF}}. \tag{49}$$

Here u_{MF} is their auxiliary function, not the electrostatic potential u in the main text. The transformed Laplace equation is

$$\sum_i \frac{1}{h_i^2 X_i f_i} \frac{d}{d\xi_i}\left(f_i \frac{dX_i}{d\xi_i}\right) = \sum_i \frac{1}{h_i^2 R f_i} \frac{\partial}{\partial \xi_i}\left(f_i \frac{\partial R}{\partial \xi_i}\right). \tag{50}$$

They take the right-hand side to be $-k_1^2/u_{\mathrm{MF}}$ in the reduction to Stäckel form. The square on R and the auxiliary function must be retained for general R. Their discussion includes bispherical and toroidal coordinates. We use only the ordinary normalization $R = u_{\mathrm{MF}} = 1$ below, for which the condition (47) on the metric tensor and the volume relation reduce to the forms needed here. The general discussion does not by itself specify a paraboloidal solution or spectrum.

Then $\sqrt{g}/g_{ii} = M_{i1} f_1 f_2 f_3$. In the divergence formula, M_{i1} and the two factors f_j with $j \neq i$ pass through the u^i derivative unchanged. Cancelling the volume factor therefore gives

$$\nabla^2 \psi = \frac{1}{S} \sum_i \frac{M_{i1}}{f_i} \frac{\partial}{\partial u^i}\left(f_i \frac{\partial X_i}{\partial u^i}\right) \prod_{j \neq i} X_j. \tag{51}$$

For the paraboloidal system, $R = u_{\mathrm{MF}} = 1$ follows directly from the metric tensor and the one-coordinate factors, including those transcribed from Morse and Feshbach p. 664. Their middle factor may be multiplied by a constant factor of unit size (a constant phase, ± 1 or $\pm i$) to make all f_i positive; the one-coordinate differential operator is unchanged.

We can now choose the one-coordinate ODEs so that they recombine correctly. This is Moon and Spencer's separated form [1, p. 6, (1.26)] and the cofactor recombination described by Morse and Feshbach [2, p. 656]. For constants $\alpha_1, \alpha_2, \alpha_3$, define $\Phi_i = \alpha_1 S_{i1} + \alpha_2 S_{i2} + \alpha_3 S_{i3}$. By (46), $\sum_i M_{i1} \Phi_i = \alpha_1 S$. If

$$\frac{1}{f_i} \frac{d}{du^i}\left(f_i \frac{dX_i}{du^i}\right) + \Phi_i(u^i) X_i = 0, \tag{52}$$

then, with $R = 1$, substitution into (51) gives $(\nabla^2 + \alpha_1)\psi = 0$. Laplace takes $\alpha_1 = 0$, Helmholtz $\alpha_1 = \kappa^2 = k^2$, exactly the convention stated below their (1.26). The second and third columns supply the two shared separation constants; the first supplies the global k^2 term. Different constants in three separate equations would not generally recombine into one equation.

What to notice. This is the reason for shared constants: the second- and third-column contributions sum to zero, whereas the first-column contribution survives. Separation works because the weights supplied by the metric tensor are precisely the cofactors that perform those cancellations.

A.3 Worked case: confocal paraboloidal coordinates

Return to $(u^1, u^2, u^3) = (\mu, \nu, \lambda)$. The following matrix is the concrete instance of the general construction. To make its entries readable, W_μ, W_ν, W_λ denote the positive quadratic products defined beside it. Moon and Spencer print [1, Table 1.11, p. 44]

$$\mathsf{S} = \begin{bmatrix} \dfrac{\mu^2}{W_\mu} & -\dfrac{1}{W_\mu} & \dfrac{\mu}{W_\mu} \\ \dfrac{\nu^2}{W_\nu} & -\dfrac{1}{W_\nu} & \dfrac{\nu}{W_\nu} \\ -\dfrac{\lambda^2}{W_\lambda} & \dfrac{1}{W_\lambda} & -\dfrac{\lambda}{W_\lambda} \end{bmatrix}, \qquad \begin{aligned} W_\mu &= (\mu - b)(\mu - c), \\ W_\nu &= (b - \nu)(c - \nu), \\ W_\lambda &= (b - \lambda)(\lambda - c). \end{aligned} \tag{53}$$

All three W's are positive on their printed intervals. Expanding gives

$$S = \frac{(\mu-\nu)(\mu-\lambda)(\lambda-\nu)}{W_\mu W_\nu W_\lambda}, \tag{54}$$

and the printed p. 45 first-column cofactors

$$M_{11} = \frac{\lambda-\nu}{W_\nu W_\lambda}, \qquad M_{21} = \frac{\mu-\lambda}{W_\mu W_\lambda}, \qquad M_{31} = \frac{\mu-\nu}{W_\mu W_\nu}. \tag{55}$$

Substitution into (47) recovers $h_\mu^2 = (\mu-\nu)(\mu-\lambda)/W_\mu$, $h_\nu^2 = (\mu-\nu)(\lambda-\nu)/W_\nu$, and $h_\lambda^2 = (\lambda-\nu)(\mu-\lambda)/W_\lambda$ of Sec. 3; for example

$$\frac{S}{M_{11}} = \frac{(\mu-\nu)(\mu-\lambda)}{W_\mu} = h_\mu^2. \tag{56}$$

Choose $f_\mu = \sqrt{W_\mu}$, $f_\nu = \sqrt{W_\nu}$, and $f_\lambda = \sqrt{W_\lambda}$. Then $g^{1/2} = S f_\mu f_\nu f_\lambda$, verifying $R = 1$ here.

Put $\alpha_1 = k^2$ and retain Moon and Spencer's names α_2, α_3. The signed product $(s-b)(s-c)$ equals W_μ for $s=\mu$, W_ν for $s=\nu$, and $-W_\lambda$ for $s=\lambda$. With these signs, Eq. (52) becomes the single form

$$(s-b)(s-c)F'' + \tfrac{1}{2}(2s-b-c)F' + (k^2 s^2 + \alpha_3 s - \alpha_2)F = 0, \tag{57}$$

where $s = \mu, \nu, \lambda$ and primes denote d/ds. The negative sign for the middle interval $c < \lambda < b$ is why the displayed handbook equation for Λ is written with an overall minus sign relative to this form. At $k = 0$, these are the Laplace equations on p. 46:

$$\begin{aligned} (\mu-b)(\mu-c)M'' + \tfrac{1}{2}[2\mu-(b+c)]M' - (\alpha_2 - \alpha_3\mu)M = 0, \\ (b-\nu)(c-\nu)N'' + \tfrac{1}{2}[2\nu-(b+c)]N' - (\alpha_2 - \alpha_3\nu)N = 0, \\ (b-\lambda)(\lambda-c)\Lambda'' - \tfrac{1}{2}[2\lambda-(b+c)]\Lambda' + (\alpha_2 - \alpha_3\lambda)\Lambda = 0. \end{aligned} \tag{58}$$

The first two follow directly and the third is -1 times the unified form. Finally, the cofactor-weight identity $\sum_i M_{i1} S_{i1} = S$ turns the first column $(\mu^2/W_\mu, \nu^2/W_\nu, -\lambda^2/W_\lambda)^{\mathsf{T}}$ into $k^2\psi$ in $(\nabla^2 + k^2)\psi = 0$. Equation (57) thus agrees with p. 47 general Helmholtz case, with $\kappa^2 = k^2$ and its λ equation again -1 times the unified form. The logarithmic solution is used in Sec. 5; the Baer specialization is noted in Sec. 4. Neither requires a different separation mechanism. These identities were verified symbolically with SymPy; see the ancillary file `check_appendix_staeckel.py`, which accompanies the arXiv version.

The Helmholtz case in Arscott's angles. For $k \neq 0$ the three separated equations are no longer Mathieu equations. With Arscott's angles (Sec. 6, Eq. (26)) each one takes the form of the three-term Hill equation, also called the Whittaker–Hill equation (a second-order equation whose coefficient of w is periodic in θ; here that coefficient contains $\cos 2\theta$ and $\cos 4\theta$, and the $\cos 4\theta$ term is absent when $k = 0$, which gives Mathieu's equation),

$$w'' + \big(\lambda_A + \mu_A \cos 2\theta - \tfrac{1}{2}k^2(b-c)^2 \cos 4\theta\big) w = 0, \tag{59}$$

with $\theta = i\alpha$, β, $\frac{1}{2}\pi + i\gamma$ for the μ, λ, ν factors, where $\lambda_A = 4\alpha_2 - 2\alpha_3(b+c) - k^2\big[(b+c)^2 + \frac{1}{2}(b-c)^2\big]$ and $\mu_A = -2(b-c)\big[\alpha_3 + k^2(b+c)\big]$ [14, (1.6)–(1.7)]. Arscott's constant c is our $b-c$, and his separation constants are written λ, μ. For $k = 0$ one has $\lambda_A = a$ and $\mu_A = -2q$, which is Eq. (25). The reduction was checked symbolically with SymPy. As printed, Arscott's Eq. (1.6c) has the opposite sign on the μ term; the sign used here follows from his Eqs. (1.1), (1.4) and (1.7), and for $k = 0$ it agrees with Eq. (4.2c) of [13].

Morse–Feshbach matrix and separation constants. Write $t_i = \xi_i^2$ and, only in this paragraph, $A = a_{\mathrm{MF}}^2$, $B = b_{\mathrm{MF}}^2$. Their p. 664 Stäckel matrix T has row

$$(T_{i1}, T_{i2}, T_{i3}) = \left(t_i, \frac{t_i}{t_i - A}, \frac{t_i}{(t_i - B)(A - B)} \right). \tag{60}$$

Its determinant divided by the first-column cofactor equals $h_i^2 = t_i \prod_{j \neq i} (t_i - t_j)/[(t_i - A)(t_i - B)]$. This formula, which also follows from differentiating their x, y, z, agrees with their printed h_1 and h_3. Their printed h_2, however, has numerator $(t_3 - t_1)(t_2 - t_3)$, whereas the correct numerator is $(t_2 - t_1)(t_2 - t_3)$. This misprint appears both in the original McGraw-Hill printing and in the Feshbach Publishing reprint. It is confined to the displayed h_2: their matrix (60) gives the correct value, and nothing else on the page depends on it. Morse and Feshbach [2, p. 656] write their separated equations as $f_i^{-1}(f_i X_i')' + \sum_j T_{ij} k_j^2 X_i = 0$, with $k_1^2 = k^2$ and separation constants k_2^2, k_3^2. The superscript 2 follows their notation; it is not an additional positivity restriction imposed here. With $(t_1, t_2, t_3) = 2(\mu, \lambda, \nu)$, $A = 2b$, $B = 2c$, their equations reduce to (57) precisely when

$$k_2^2 = \frac{2(-\alpha_2 + b\alpha_3 + b^2 k^2)}{b - c}, \qquad k_3^2 = 4(\alpha_2 - c\alpha_3 - c^2 k^2). \tag{61}$$

The first column of their matrix multiplies k_1^2, not a second separation constant. The matrix and the Jacobian of the coordinates (the determinant of the derivatives of x, y, z with respect to the coordinates) therefore fix both the names and signs in this dictionary. At $k = 0$ it gives the Laplace constants. The full matrix transformation, volume factors and ODE reduction were verified symbolically with SymPy; see the ancillary file `check_11_mf664.py`.

B Eisenhart's classification and the paraboloidal case

Appendix A shows how one Stäckel matrix produces separated equations. This appendix asks a broader question: where does that example fit among all orthogonal separable systems in ordinary three-dimensional space? Stäckel supplied a general separation framework; Eisenhart specialized it to Euclidean space and classified the resulting coordinate systems. His Type IV_2 is the paraboloidal system used in this note.

The historical discussion below is optional on a first reading. The explicit notation map at the end is useful whenever comparing sources. In this appendix E^3 means Euclidean three-dimensional space, not a new physical model. Every page citation to Eisenhart below was checked against the Internet Archive scan of *Annals of Mathematics* (2) **35** (1934), no. 2.[11]

B.1 From Stäckel (1891) to Eisenhart (1934)

The Hamilton–Jacobi equation is a first-order equation for a classical action function ϕ. Its natural separated ansatz is a *sum*, in contrast to the product used for Laplace's equation. Eisenhart recalls that Stäckel determined in 1891 the scale factors H_i for which a Hamilton–Jacobi equation separates. In Eisenhart's notation its kinetic part has the schematic form

$$\text{(A)} \qquad \sum_i \frac{1}{H_i^2} \Big(\frac{\partial \phi}{\partial x_i} \Big)^2 + \cdots = 0$$

and the separated action is $\phi = \sum_i X_i(x_i)$. The dots stand for the remaining terms of Eisenhart's equation, not an additional equation to be solved here. His x_i are curvilinear labels,

[11] Internet Archive item `sim_annals-of-mathematics_1934-04_35_2`.

not the Cartesian x, y, z used later. He also recalls the 1893 result that the same metric tensor, $ds^2 = \sum_i H_i^2\, dx_i^2$, has $n-1$ independent quadratic constants of geodesic motion (quantities that stay constant along a geodesic, are quadratic in the momenta, and are independent of the energy, which is itself conserved) besides the energy integral. Here n is the dimension and a geodesic is a locally straight path for that metric tensor [3, p. 284].[12] Eisenhart's Sections 1–2 also establish a converse, subject to smoothness assumptions: suitable quadratic constants of motion determine a metric tensor of Stäckel form [3, pp. 284, 289]. More precisely, their common orthogonal directions must be normals to coordinate surfaces. We cite that result rather than reproduce its proof.

A second issue arises for wave equations. Hamilton–Jacobi separation concerns first derivatives, whereas Laplace- and Schrödinger-type equations contain second derivatives and the volume factor. Eisenhart records Robertson's additional condition (C), and shows that it is equivalent to $R_{ij} = 0$ for $i \neq j$ in the separating coordinates [3, pp. 284, 289–291]. Here R_{ij} are components of the Ricci curvature tensor, a geometric quantity derived from the metric tensor. They are unrelated to the prefactor R in Appendix A. In Euclidean space the curvature tensor vanishes. Appendix A verifies the required $R = 1$ volume-factor identity directly for our example; no tensor calculation is needed to use it.

What to notice. Stäckel's framework is not restricted to flat space. Eisenhart's Euclidean classification is a specialization, not a claim that curved-space Stäckel systems do not exist.

B.2 Orthogonal Stäckel systems in E^3

Eisenhart writes an orthogonal metric tensor, $ds^2 = \sum_i e_i H_i^2\, dx_i^2$ with no cross terms, where e_i are signs (all $+1$ in the Euclidean case considered here), and defines the Stäckel form by n^2 functions $\varphi_{ij}(x_i)$, each depending only on the coordinate of its row, with $\varphi = \det(\varphi_{ij}) \neq 0$ and cofactors φ^{i1} of the entries φ_{i1}, through [3, p. 287, (2.1)]

$$H_i^2 = \frac{\varphi}{\varphi^{i1}}. \tag{62}$$

This is the same relation as $g_{ii} = S/M_{i1}$ in Appendix A, with $(\varphi_{ij}, \varphi, \varphi^{i1})$ corresponding to (S_{ij}, S, M_{i1}). He proves that the geodesic-integral hypotheses force each φ_{ij} to depend on x_i alone, and states the necessary and sufficient conditions for a metric tensor to be put in Stäckel form [3, p. 289].

To select ordinary Euclidean geometry from the larger Stäckel family, he imposes vanishing curvature. This is not an extra approximation to the physics: curving the coordinate surfaces does not curve the ambient space. For example, spherical coordinates describe flat Euclidean space despite their nonconstant scale factors.

With this restriction he reduces the possible H_i in E^3 to four canonical families (standard algebraic forms) (3.21)–(3.24), and concludes that his Schrödinger-type equation (B) separates for $n = 3$ if and only if the H_i are of one of those forms [3, p. 295]. The four families are developed as Types I–IV in §§4–7 (Cartesian and circular cylindrical; polar and spheroidal; systems containing a family of planes through a common line; and the full confocal-quadric cases). The classification theorem on p. 301 then reads, in substance:[13]

[12] Eisenhart's footnote 1 on p. 284 cites only "Habilitationsschrift, Halle." We identify this with Stäckel's printed Halle habilitation [6]; we do not quote internal page numbers of that work here. His footnote 2 cites the 1893 *Comptes Rendus* note, vol. 116, pp. 485–487.

[13] Italicized statement on Eisenhart p. 301; wording checked against the scan.

> A necessary and sufficient condition that a triply orthogonal system of surfaces in Euclidean 3-space be a coordinate system in terms of which the fundamental quadratic form is such that the variables are separated in the corresponding Hamilton–Jacobi equation and the Laplace equation is that they be any system of confocal quadrics, including the cases when one or more families of the system consists of planes.

Here a *quadric* is a surface defined by a second-degree Cartesian equation, such as an ellipsoid, hyperboloid or paraboloid. Planar degenerations include the familiar coordinate planes. In modern terms: three families of surfaces that cross at right angles; the "fundamental quadratic form" is ds^2; "confocal" for quadrics means sharing foci in the sense of Sec. 2.1 for the paraboloids; and the "planar degenerations" are the limiting cases in which one or more families consist of planes. Thus, within the orthogonal Stäckel setting of the theorem, the systems in E^3 are precisely the confocal quadrics and their planar degenerations [3, p. 301].

B.3 Paraboloidal coordinates as Type IV_2

Type IV starts from Eisenhart's general form (3.24) of the metric tensor. The degree and roots of its polynomial f distinguish the subcases. When the cubic $f(x) = 0$ has three distinct roots one obtains ellipsoidal (confocal ellipsoid/hyperboloid) coordinates, labeled (IV_1) on p. 300. Setting the cubic coefficient a_0 to zero in (7.4) leaves a quadratic. This gives

$$(\mathrm{IV}_2) \qquad H_i^2 = \frac{(x_i - x_j)(x_i - x_k)}{f(x_i)}, \qquad f(x_i) = 4(a - x_i)(b - x_i), \tag{63}$$

Here a, b are Eisenhart's parameters, not yet Moon and Spencer's. The coordinate ordering is $x_1 > b > x_2 > a > x_3$ [3, p. 301]. The *Cartesian form* of the coordinates, meaning the formulas that give Cartesian position in terms of those labels, is [3, p. 301, (7.6)]

$$\begin{aligned} x &= \frac{x_1 + x_2 + x_3 - a - b}{2}, \\ y^2 &= \frac{(a - x_1)(a - x_2)(a - x_3)}{b - a}, \\ z^2 &= \frac{(b - x_1)(b - x_2)(b - x_3)}{a - b}. \end{aligned} \tag{64}$$

Because these formulas give y^2 and z^2, each set of labels corresponds to up to four points, mirror images in the planes $y = 0$ and $z = 0$; fixing the signs of y and z selects one. This is the same four-fold labeling as in Sec. 2.1, where the two transverse coordinates are Moon and Spencer's x, y (Eq. (68) below gives the correspondence); Sec. 2.2 treats the planes themselves. The surfaces $x_i = \text{const}$ are the confocal paraboloids [3, p. 301, (7.7)]. The identity implied by (64),

$$\frac{y^2}{a - x_i} + \frac{z^2}{b - x_i} = 2x - x_i, \tag{65}$$

was verified symbolically from (64); it is the form used below.[14] Eisenhart excludes $a = b$ for this form [3, p. 301]; the displayed formulas themselves have zero denominators there. We do not infer a limiting coordinate system by simply substituting equal parameters. A contemporaneous Letter to

[14] On the Internet Archive microfilm of p. 301, the printed right-hand side of (7.7) reads $x_i - 2x$. Direct expansion of (64) yields instead $2x - x_i$ (symbolic identity, checked for each $i = 1, 2, 3$). We therefore cite (7.7) as identifying the surfaces as confocal paraboloids and use the algebraically forced identity (65).

the Editor lists the same eleven real orthogonal types for the three-dimensional Schrödinger equation, with the formulas for Cartesian position [4]; its type (XI), labeled there "confocal parabolic coordinates," reproduces (63)–(64) exactly (Ann. Math. Type IV_2), the only notation difference being "parabolic" versus the "paraboloidal" surfaces named on p. 301 of the Annals paper. Arfken also points readers to this 1934 Physical Review paper when introducing the eleven systems separating Helmholtz's equation [10, p. 72; see also p. 78 for $k^2 \neq 0$]. Miller [17, Table 14, p. 164], and earlier Boyer, Kalnins and Miller [16, Table 1], list the same eleven systems for Helmholtz's equation; Miller states that there are no nontrivial R-separable solutions in that case [17, p. 163]. A solution is R-separable when it is a fixed known function R of the coordinates times a product of functions of one variable each. Ordinary separation is the case $R = 1$. The remaining case is called nontrivial when R cannot itself be written as a product of one-variable factors [16, pp. 35–36, (0.3)]. In those lists the paraboloidal system is number 9, not number 11: the title's "eleventh system" follows Eisenhart's type (XI) in the 1934 letter. For Laplace's equation the same eleven remain ordinarily separable. Six further systems, whose surfaces are confocal cyclides (quartic surfaces, given by $a(x^2 + y^2 + z^2)^2 + P(x, y, z) = 0$ with P a polynomial of degree two; for $a = 0$ such a surface is a quadric, so the confocal quadrics are the special case $a = 0$), are purely R-separable and do not separate Helmholtz's equation, giving seventeen systems in all [17, Table 17, pp. 208–212], [16, §6]. The original list of seventeen is due to Böcher (1894), which we have not checked. Our system is one of the eleven, not one of the extra six.

The Stäckel functions for these cases are recorded as [3, p. 301]

$$\varphi_{i1} = \frac{x_i^2}{f(x_i)}, \qquad \varphi_{i2} = \frac{1}{f(x_i)}, \qquad \varphi_{i3} = \frac{x_i}{f(x_i)}. \tag{66}$$

B.4 Map to Moon and Spencer, and to Appendix A

Keep the axes separate. Eisenhart's axial Cartesian coordinate is x, whereas Moon and Spencer's is z. To avoid confusing these names, subscripts E and MS below identify the source's Cartesian frame. This is distinct from the relabeling of curvilinear coordinates.

Moon and Spencer's parameters (b, c) and coordinates (μ, ν, λ) with $\mu > b > \lambda > c > \nu$ match Eisenhart's (b, a) and (x_1, x_2, x_3) under

$$a \leftrightarrow c, \qquad (x_1, x_2, x_3) \leftrightarrow (\mu, \lambda, \nu), \tag{67}$$

so that Eisenhart's middle coordinate is the hyperbolic-paraboloid label (Moon–Spencer λ, Morse–Feshbach ξ_2). The Cartesian frames differ by a permutation and a constant scale: with (67),

$$x_{\mathrm{E}} = \tfrac{1}{2} z_{\mathrm{MS}}, \qquad 4\, y_{\mathrm{E}}^2 = y_{\mathrm{MS}}^2, \qquad 4\, z_{\mathrm{E}}^2 = x_{\mathrm{MS}}^2, \tag{68}$$

and consequently

$$H_i^2 = \tfrac{1}{4} h_\sigma^2 \tag{69}$$

for the corresponding Moon–Spencer scale factors h_μ, h_λ, h_ν of Sec. 3. Both (68) and (69) are symbolic identities; see the ancillary file `check_08_eisenhart_map.py`.

Under the same identification, Eisenhart's f is tied to Moon and Spencer's W's by

$$f(\mu) = 4W_\mu, \qquad f(\nu) = 4W_\nu, \qquad f(\lambda) = -4W_\lambda, \tag{70}$$

The apparent row-sign difference is already accounted for by $f(\lambda) < 0$. After putting the rows in Moon and Spencer's order (μ, ν, λ), the matrix of Eisenhart's functions is exactly $\frac{1}{4}\mathsf{S}\,\mathrm{diag}(1, -1, 1)$.

Thus the second column has the opposite sign, and all entries have the common factor 1/4. The column sign changes the convention for its separation constant, not the metric tensor. The common factor gives $H_i^2 = h_\sigma^2/4$, as required by the Cartesian scale change. An independent row-sign reversal would, in general, change the associated component of the metric tensor; it is not needed in this comparison.

Morse and Feshbach's square-root coordinates $(\xi_1, \xi_2, \xi_3) = (\sqrt{2\mu}, \sqrt{2\lambda}, \sqrt{2\nu})$ (with their $a^2 = 2b$, $b_{\mathrm{MF}}^2 = 2c$) therefore sit on the same Type IV_2 geometry, again with the second label equal to Eisenhart's middle coordinate.[15]

What to notice. These are not three different physical geometries. Eisenhart, Moon–Spencer and Morse–Feshbach describe the same confocal paraboloidal families using different labels and scales. Matching a formula therefore requires checking both the coordinate transformation and the axis convention, not just recognizing the surface names.

Thus the confocal paraboloidal system of the present note is Eisenhart's Type IV_2 inside his confocal-quadric classification, written in Moon and Spencer's axial convention and parameter names. Appendix A's matrix (53) is the corresponding Stäckel matrix in that convention.

C Proof of the far-field law

This appendix proves Theorem 7.1 in full. The sketch in Sec. 7.5 replaced several quantities by their small-argument forms; here every replacement is bounded by an explicit inequality. The only external facts used are standard properties of J_0, K_0, K_1, and the gamma function, cited by equation number from the NIST Digital Library of Mathematical Functions [25]. Every inequality and constant below was also checked numerically with `mpmath` at 30 significant digits.

Plan. After the substitution $t = \lambda u$ of (41), $V = u^{-2} I$ with

$$I = \int_0^\infty t\, \tilde{a}(t/u)\, J_0(\kappa t)\, \frac{K_0(t)}{K_0(\varepsilon t)}\, dt, \qquad \varepsilon = \frac{u_0}{u}. \tag{71}$$

Four things are thrown away in the sketch: (a) the change from $\tilde{a}(t/u)$ to $\tilde{a}(0)$; (b) the large-t part of the integral, where $K_0(t)$ is exponentially small; (c) the error made when $1/K_0(\varepsilon t)$ is replaced by its expansion about a large logarithm; and (d) any question about the oscillating factor $J_0(\kappa t)$. We cut the integral at

$$T = \sqrt{u/u_0} = \varepsilon^{-1/2}. \tag{72}$$

For $t \le T$ the argument $\varepsilon t \le \sqrt{\varepsilon}$ is small, so the logarithm $\ln(2/(\varepsilon t))$ is at least about $\frac{1}{2}\ln(u/u_0)$. For $t > T$ the factor $K_0(t)$ is smaller than e^{-T}, which is far smaller than any power of $1/\ln u$. The difficult values $t \sim u/u_0$, where εt is of order one and the logarithm is not large, lie deep inside the discarded tail, so no expansion is ever used there.

C.1 Hypotheses and notation

Hypothesis (H). The electrode data $f(v)$ are axisymmetric and satisfy

$$M_1 = \int_0^\infty v\, |f(v)|\, dv < \infty, \qquad M_3 = \int_0^\infty v^3\, |f(v)|\, dv < \infty. \tag{73}$$

[15] The p. 664 matrix and the p. 665 general R-separation formulas have now been transcribed from the author's photographs and checked algebraically. Their general convention on pp. 655–656 identifies the printed constants as k_1^2, k_2^2, k_3^2; Eq. (61) gives their verified dictionary to Moon and Spencer.

The electrode parameter $u_0 > 0$ is fixed. Directions are restricted to $0 \le \kappa \le K$ for some fixed K; in terms of the polar angle from the focus, this is the closed cone $0 \le \theta \le 2\arctan K < \pi$. No condition $\tilde{a}(0) \neq 0$ is needed. When $\tilde{a}(0) = 0$ the result is an upper bound on V; see Remark 2.

For the Gaussian $f = e^{-v^2}$ one has $M_1 = M_3 = 1/2$.

Notation. $L = \ln(u/u_0)$, so $\varepsilon = e^{-L}$. γ is Euler's constant and $c_0 = \ln 2 - \gamma = 0.11593\ldots$. $\beta = \ln(1+\kappa^2)$ and $A = L + \beta$; since $R = u^2(1+\kappa^2)$, $A = \ln\bigl(R/(uu_0)\bigr)$, the logarithm in (40). We write $D(t) = K_0(\varepsilon t)$ for the denominator,

$$\rho(z) = K_0(z) + \ln(z/2) + \gamma, \tag{74}$$

for the difference between K_0 and its leading logarithm, and $h(t) = c_0 - \beta - \ln t$. Then, exactly,

$$D(t) - A = h(t) + \rho(\varepsilon t). \tag{75}$$

Finally, $b_K = c_0 + \ln(1+K^2)$, so that $|c_0 - \beta| \le b_K$ for $0 \le \kappa \le K$.

C.2 Standard facts used

(F1) $|J_0(x)| \le 1$ for real x [25, 10.14.1]. Also $J_0' = -J_1$ [25, 10.6.3] and $|J_1(x)| \le |x|/2$ [25, 10.14.4]. Integrating gives $|1 - J_0(x)| \le x^2/4$.

(F2) K_0 is positive and decreasing on $(0,\infty)$ [25, §10.37].

(F3) $K_0(x) < K_{1/2}(x)$ and $K_1(x) < K_{3/2}(x)$ for $x > 0$ [25, 10.37.1]. Here $K_{1/2}(x) = \sqrt{\pi/(2x)}\,e^{-x}$ [25, 10.39.2], and the recurrence [25, 10.29.1] gives $K_{3/2}(x) = \sqrt{\pi/(2x)}\,e^{-x}(1 + 1/x)$.

(F4) $\frac{d}{dt}\bigl(tK_1(t)\bigr) = -tK_0(t)$ [25, 10.29.4], so $\int_T^\infty tK_0(t)\,dt = TK_1(T)$.

(F5) $K_0(z) = -\bigl(\ln(z/2)+\gamma\bigr)I_0(z) + \sum_{k\ge1} H_k\,(z^2/4)^k/(k!)^2$, with $H_k = 1 + \frac12 + \cdots + \frac1k$ [25, 10.31.2], and $I_0(z) = \sum_{k\ge0}(z^2/4)^k/(k!)^2$ [25, 10.25.2].

(F6) $\int_0^\infty t^{s-1}K_0(t)\,dt = 2^{s-2}[\Gamma(s/2)]^2$ for $\operatorname{Re} s > 0$ [25, 10.43.19]. In particular $\int_0^\infty tK_0\,dt = 1$ and $\int_0^\infty t^3K_0\,dt = 4$.

(F7) $J_0(x) = \sum_{n\ge0}(-1)^n(x^2/4)^n/(n!)^2$ [25, 10.2.2], and $|J_0(z)| \le e^{|\operatorname{Im} z|}$ for complex z [25, 10.14.3].

C.3 Four lemmas

Lemma C.1 (the two exact moments). *In plain words: the J_0-weighted integral of $tK_0(t)$ is exactly $1/(1+\kappa^2)$, and choosing $\beta = \ln(1+\kappa^2)$ makes the first logarithmic correction vanish exactly.* For all real $\kappa \ge 0$,

$$m_0(\kappa) = \int_0^\infty tJ_0(\kappa t)K_0(t)\,dt = \frac{1}{1+\kappa^2}, \qquad \int_0^\infty tJ_0(\kappa t)K_0(t)\,h(t)\,dt = 0. \tag{76}$$

Proof. Let $M(s,\kappa) = \int_0^\infty t^{s-1}J_0(\kappa t)K_0(t)\,dt$ for $\operatorname{Re} s > 0$. Take first $0 \le \kappa < 1$. Insert the series (F7) and integrate term by term using (F6). This is allowed because the series of absolute values gives $\int_0^\infty t^{\operatorname{Re} s - 1}I_0(\kappa t)K_0(t)\,dt$, which is finite for $\kappa < 1$, since $I_0(\kappa t)K_0(t)$ decays like $e^{-(1-\kappa)t}$. The result is

$$M(s,\kappa) = 2^{s-2}\sum_{n\ge0}\frac{[\Gamma(s/2+n)]^2}{(n!)^2}(-\kappa^2)^n. \tag{77}$$

At $s=2$ this is $\sum_n(-\kappa^2)^n = 1/(1+\kappa^2)$. Differentiating (77) in s at $s=2$ (again term by term, dominated by $\int_0^\infty t|\ln t| I_0(\kappa t)K_0(t)\,dt$) and using $\psi(n+1) = -\gamma + H_n$ [25, §5.4] gives

$$m_1 = \int_0^\infty t \ln t\, J_0(\kappa t)K_0(t)\,dt = \sum_{n\ge 0}(c_0 + H_n)(-\kappa^2)^n = \frac{c_0 - \ln(1+\kappa^2)}{1+\kappa^2}, \tag{78}$$

by the generating function $\sum_n H_n y^n = -\ln(1-y)/(1-y)$ for $|y|<1$. Hence $\int tJ_0K_0\,h\,dt = (c_0-\beta)m_0 - m_1 = 0$. For $\kappa \ge 1$, analytic continuation finishes the proof (two analytic functions that agree on an interval agree throughout any connected region where both are defined). By (F7), (F2) and (F3), m_0 and m_1 are analytic functions of κ in the strip $|\operatorname{Im}\kappa| < 1$, because there the integrand is bounded by a constant times $t(1+|\ln t|)K_0(t)e^{|\operatorname{Im}\kappa| t}$. The right-hand sides $1/(1+\kappa^2)$ and $(c_0 - \ln(1+\kappa^2))/(1+\kappa^2)$ are also analytic in that strip. The two sides agree for $0 \le \kappa < 1$, so they agree for all real κ. □

Numerically, quadrature reproduces m_0 and $\beta = c_0 - m_1/m_0$ to twenty digits at $\kappa = 0, \frac{1}{2}, 1, 2, 5$.

Lemma C.2 (K_0 near zero). *In plain words: $K_0(z)$ is never below its leading logarithm, and on $0 < z \le 1$ it exceeds it by at most a multiple of $z^2\ln(1/z)$.* For all $z > 0$,

$$K_0(z) \ge \ln(2/z) - \gamma. \tag{79}$$

For $0 < z \le 1$,

$$0 \le \rho(z) \le z^2\big[a_1\big(\ln(2/z) - \gamma\big) + a_2\big] \le \rho_1, \tag{80}$$

with $a_1 = I_0(1) - 1 = 0.26607\ldots$, $a_2 = \sum_{k\ge1} H_k 4^{-k}/(k!)^2 = 0.27425\ldots$, and $\rho_1 = \rho(1) = a_1c_0 + a_2 = 0.30509\ldots$.

Proof. By (F5), $\rho(z) = \big(\ln(2/z)-\gamma\big)\big(I_0(z)-1\big) + \sum_{k\ge1} H_k(z^2/4)^k/(k!)^2$. For $z \le 2e^{-\gamma} = 1.12\ldots$ both terms are non-negative, so $\rho \ge 0$, which is (79). For larger z the right side of (79) is negative while $K_0 > 0$. For $0 < z \le 1$ we have $(z^2/4)^k \le z^2\,4^{-k}$ when $k \ge 1$, so $I_0(z) - 1 \le a_1 z^2$ and the second sum is at most $a_2 z^2$. Finally, $z^2\ln(2/z)$ increases on $(0,1]$, so the bracketed bound is largest at $z = 1$, where it equals $\rho(1)$. □

Lemma C.3 (tails). *In plain words: beyond $t = T$ the weight $K_0(t)$ contributes only an amount of order e^{-T}.* For $T \ge 1$,

$$\int_T^\infty tK_0(t)\,dt = TK_1(T) \le \sqrt{2\pi T}\,e^{-T}, \qquad \int_T^\infty t^2K_0(t)\,dt \le 5\sqrt{\pi/2}\,T^2e^{-T}. \tag{81}$$

Proof. The first part is (F4) followed by (F3), using $1 + 1/T \le 2$. For the second, (F3) gives $t^2K_0(t) \le \sqrt{\pi/2}\,t^{3/2}e^{-t} \le \sqrt{\pi/2}\,t^2e^{-t}$ for $t \ge 1$. Also $\int_T^\infty t^2e^{-t}\,dt = (T^2+2T+2)e^{-T} \le 5T^2e^{-T}$. □

Lemma C.4 (the data). *In plain words: under (H), $\tilde a$ is bounded and flat to second order at $\lambda = 0$.* For all $\lambda \ge 0$, $|\tilde a(\lambda)| \le M_1$ and $|\tilde a(\lambda) - \tilde a(0)| \le M_3\lambda^2/4$.

Proof. Use $|J_0| \le 1$ and $|1 - J_0(\lambda v)| \le \lambda^2v^2/4$ from (F1) in $\tilde a(\lambda) - \tilde a(0) = \int_0^\infty f(v)\,[J_0(\lambda v) - 1]\,v\,dv$. □

C.4 The theorem with explicit bounds

Theorem C.5 (precise form of Theorem 7.1). *Assume (H), and let* $0 \le \kappa \le K$ *and* $u \ge e\,u_0$ *(so* $L \ge 1$*). Then*

$$\Big| V - \frac{\tilde a(0)}{R\ln\big(R/(uu_0)\big)} \Big| \le \frac{1+\kappa^2}{R}\Big[\frac{2|\tilde a(0)|\,N_2(K)}{L^3} + \mathcal{E}(u)\Big], \tag{82}$$

where

$$N_2(K) = \int_0^\infty tK_0(t)\big(b_K + |\ln t| + \rho_1\big)^2 dt \tag{83}$$

and

$$\begin{aligned}\mathcal{E}(u) = {}& \big[(1+b_K)|\tilde a(0)| + M_1\big]\sqrt{2\pi T}\,e^{-T} + 5\sqrt{\pi/2}\,|\tilde a(0)|\,T^2 e^{-T} \\ & + \frac{u_0^2}{u^2}\,|\tilde a(0)|\big[4a_1(L+c_0) + a_1 N_{\ln} + 4a_2\big] + \frac{2M_3}{u^2 L},\end{aligned} \tag{84}$$

with $T = \sqrt{u/u_0}$ *and* $N_{\ln} = \int_0^\infty t^3 K_0(t)|\ln t|\,dt = 4.5618\ldots$ Numerically $N_2(0) = 1.6246$, $N_2(1) = 3.6953$, $N_2(2) = 7.9074$.

Every term of $\mathcal{E}(u)$ is $O(u^{-2}\ln u)$ or $O(u\,e^{-\sqrt{u/u_0}})$, so $L^3\mathcal{E}(u) \to 0$. Since $L = \ln u - \ln u_0$, (82) is the statement $V = \tilde a(0)/[R\ln(R/(uu_0))] + O\big(1/(R(\ln u)^3)\big)$ of Theorem 7.1, uniformly for $0 \le \kappa \le K$.

Proof. The proof has five steps. Steps 1 to 4 handle items (d), (b), (a) and (c) of the plan, in that order. Step 5 collects the bounds.

Step 1: absolute convergence (item d). For $t > 0$ we have $\varepsilon t < t$, so $K_0(t)/K_0(\varepsilon t) \le 1$ by (F2). With $|J_0| \le 1$ and Lemma C.4, the integrand of (71) is bounded in absolute value by $M_1\,tK_0(t)$, which is integrable by (F6). Every integral below is likewise absolutely convergent. The oscillation of $J_0(\kappa t)$ is never used to obtain cancellation in an error bound. It enters only through $|J_0| \le 1$ and through the two exact identities of Lemma C.1.

Step 2: the large-t tail (item b). Split $I = I_< + I_>$ at $t = T$. By Step 1 and Lemma C.3,

$$|I_>| \le M_1 \int_T^\infty tK_0(t)\,dt \le M_1\sqrt{2\pi T}\,e^{-T}. \tag{85}$$

Step 3: replacing $\tilde a(t/u)$ *by* $\tilde a(0)$ *(item a).* On $0 < t \le T$, (F2) and (79) give

$$D(t) \ge K_0(\varepsilon T) = K_0(\sqrt{\varepsilon}) \ge \tfrac12 L + c_0 > \tfrac12 L. \tag{86}$$

So the denominator is large on the whole kept range. Write $I_< = \tilde a(0)J_T + E_a$, with $J_T = \int_0^T tJ_0(\kappa t)K_0(t)/D(t)\,dt$. By Lemma C.4, (86) and (F6),

$$|E_a| \le \int_0^T t\,\frac{M_3 t^2}{4u^2}\,K_0(t)\,\frac{2}{L}\,dt \le \frac{2M_3}{u^2 L}. \tag{87}$$

Step 4: the expansion of $1/D$ *(item c).* For any $D > 0$ and $A > 0$ the algebraic identity

$$\frac{1}{D} = \frac{1}{A} - \frac{D-A}{A^2} + \frac{(D-A)^2}{A^2 D} \tag{88}$$

is exact. It is applied with $D = K_0(\varepsilon t)$, which is strictly positive for every t by (F2). So no truncated logarithm is ever divided by, and the sign or possible zero of $\ln(2/(\varepsilon t))$ near $t \sim u/u_0$ plays no role.

That range lies in the tail of Step 2 anyway, because $T = \sqrt{u/u_0} \ll u/u_0$. Inserting (88) and (75) into J_T gives

$$J_T = \frac{m_0 - \tau_0}{A} + \frac{\tau_1 - P}{A^2} + Q, \tag{89}$$

where

$$\tau_0 = \int_T^\infty tJ_0K_0\,dt, \qquad \tau_1 = \int_T^\infty tJ_0K_0\,h\,dt,$$
$$P = \int_0^T tJ_0K_0\,\rho(\varepsilon t)\,dt, \qquad Q = \frac{1}{A^2}\int_0^T tJ_0K_0\,\frac{(D-A)^2}{D}\,dt. \tag{90}$$

Here both identities of Lemma C.1 were used to rewrite $\int_0^T = \int_0^\infty - \int_T^\infty$. We bound each piece in turn.

τ_0 and τ_1. By Lemma C.3, $|\tau_0| \le \sqrt{2\pi T}\,e^{-T}$. For $t \ge T \ge 1$ we have $|h(t)| \le b_K + t$, since $0 \le \ln t \le t$. So $|\tau_1| \le b_K\sqrt{2\pi T}\,e^{-T} + 5\sqrt{\pi/2}\,T^2e^{-T}$.

P. On $t \le T$ we have $\varepsilon t \le \sqrt{\varepsilon} \le 1$. Lemma C.2 then applies with $\ln\bigl(2/(\varepsilon t)\bigr) - \gamma = L + c_0 - \ln t$, which gives

$$|P| \le \varepsilon^2 \int_0^\infty t^3K_0(t)\bigl[a_1(L + c_0 + |\ln t|) + a_2\bigr]dt = \frac{u_0^2}{u^2}\bigl[4a_1(L + c_0) + a_1N_{\ln} + 4a_2\bigr]. \tag{91}$$

Q, the true error term. On $0 < t \le T$, (75) and Lemma C.2 give $|D - A| \le |c_0 - \beta| + |\ln t| + \rho_1 \le b_K + |\ln t| + \rho_1$, and (86) gives $1/D < 2/L$. With $A \ge L$ (because $\beta \ge 0$),

$$|Q| \le \frac{2}{L\,A^2}\,N_2(K) \le \frac{2N_2(K)}{L^3}. \tag{92}$$

Small t causes no difficulty. There $|\ln t|$ is large, but the weight $tK_0(t)(\ln t)^2 \sim t|\ln t|^3$ is integrable at 0, and D is even larger there.

Step 5: assembly. From Steps 2 to 4, $I - \tilde a(0)m_0/A = \tilde a(0)\bigl[-\tau_0/A + (\tau_1 - P)/A^2 + Q\bigr] + E_a + I_>$. Bound each term as above, and use $A \ge 1$. Then multiply by $u^{-2} = (1+\kappa^2)/R$. Because $u^{-2}m_0/A = 1/(RA) = 1/\bigl(R\ln(R/(uu_0))\bigr)$, this gives (82). □

Remark 1 (the order $1/(\ln u)^3$ cannot be improved in general). By Corollary C.6, when $\tilde a(0) \ne 0$ the leading part of the error is $\tilde a(0)m_0\mu_2(\kappa)/A^3$. On the axis $\mu_2(0) = \pi^2/12 \ne 0$, so there the error is of exact order $1/(R(\ln u)^3)$. Numerically μ_2 changes sign between $\kappa = 1$ and $\kappa = 2$ ($\mu_2(1) = 0.411$, $\mu_2(2) = -0.363$), so along one particular direction the error is of smaller order. No better remainder holds uniformly in a cone that contains the axis.

Remark 2 (data with $\tilde a(0) = 0$). If $\tilde a(0) = \int_0^\infty f(v)\,v\,dv = 0$, then (82) reads $|V| \le (1+\kappa^2)R^{-1}\bigl[2M_3/(u^2L) + M_1\sqrt{2\pi T}\,e^{-T}\bigr]$. In the cone $0 \le \kappa \le K$ one has $u^2 = R/(1+\kappa^2)$, so this is $V = O\bigl(1/(R^2\ln R)\bigr)$. That is an upper bound only; we have not determined the exact rate in this case.

Remark 3 (what is not claimed). The constants grow with K: $N_2(K)$ grows like $(\ln K)^2$, and the prefactor contains $1 + \kappa^2$. So the statement is uniform only on closed cones $\theta \le \theta_1 < \pi$. We make no claim about uniformity as $\theta \to \pi$, where the rays approach the far sheets of the electrode. The theorem concerns the Hankel representation (39) of the solution, taken as given from Sec. 7.

Corollary C.6 (two-term law, used in Table 4). *Assume (H), $\tilde{a}(0) \neq 0$, and $0 \le \kappa \le K$. Then*

$$\frac{V\,R\ln\big(R/(uu_0)\big)}{\tilde{a}(0)} = 1 + \frac{\mu_2(\kappa)}{\big(\ln(R/(uu_0))\big)^2} + O\Big(\frac{1}{(\ln u)^3}\Big), \tag{93}$$

where $\mu_2(\kappa) = (1+\kappa^2)\int_0^\infty tJ_0(\kappa t)K_0(t)\,h(t)^2\,dt$. On the axis $\mu_2(0) = \pi^2/12$.

Proof. Apply the identity $1/D = 1/A - (D-A)/A^2 + (D-A)^2/A^3 - (D-A)^3/(A^3D)$ in place of (88). The new last term is bounded exactly as Q was, by $2N_3(K)/L^4$, with $N_3(K) = \int_0^\infty tK_0(t)(b_K + |\ln t| + \rho_1)^3 dt$. In the new middle term, $(1/A^3)\int_0^T tJ_0K_0(D-A)^2dt$, replace $(D-A)^2$ by h^2. The difference $2h\rho + \rho^2$ is bounded through Lemma C.2 by a constant times $\varepsilon^2 L^2$. Then extend $\int_0^T$ to $\int_0^\infty$, at a cost of order T^3e^{-T} by (F3). All other pieces are as in Theorem C.5. Dividing by $\tilde{a}(0)m_0/A$ gives (93). On the axis, $M(s,0) = 2^{s-2}[\Gamma(s/2)]^2$ by (F6), and $\mu_2(0) = \partial_s^2 \ln M(s,0)|_{s=2} = \frac{1}{2}\psi'(1) = \pi^2/12$ by [25, 5.15.2]. □

Off the axis we evaluated μ_2 only numerically: $\mu_2(1) = 0.4112335167$, which agrees with $\pi^2/24$ to the fifteen digits computed. We have not proved that closed form.

C.5 Numerical check of the bounds

For the Gaussian data ($\tilde{a}(0) = M_1 = M_3 = 1/2$, $u_0 = \sqrt{5}$), we computed I by direct quadrature for $L = 1, 2, 3, 5, 8, 12, 20$ (so u up to about 10^9) at $\kappa = 0$ and $\kappa = 1$. In every case the actual error $|I - \tilde{a}(0)m_0/A|$ was below the full bound in Step 5, and the directly computed Q was below (92). The bound is conservative but has the correct order in L. For $L \ge 8$ it exceeds the actual error by a factor of about 4 on the axis and about 45 to 60 at $\kappa = 1$. On the axis, L^2 times the relative error $|IA/(\tilde{a}(0)m_0) - 1|$ is 0.783, 0.789 and 0.799 at $L = 8, 12, 20$, approaching $\mu_2(0) = \pi^2/12 = 0.822$ as Corollary C.6 predicts. The bound (86) was also checked: the minimum of D on $[0,T]$ exceeds $L/2$ in every case. For Corollary C.6, L^3 times the difference between the computed ratio and $1 + \mu_2/A^2$ stays bounded, between -0.08 and -0.75, for $L = 3$ to 30 at $\kappa = 0, 1$, as an $O(1/L^3)$ remainder should. The checks are in the ancillary files `rigor_checks.py` and `rigor_checks_twoterm.py`, which accompany the source deposit.

Acknowledgments

Drafting, symbolic and numerical checks (using `sympy` and `mpmath`), and figures were prepared with the assistance of an AI tool. The derivations and comparisons were checked against Moon and Spencer pp. 1–9 and Table 1.11, pp. 44–48; Morse and Feshbach pp. 655–656 and 664–665; Arfken's second edition, pp. 119–120; the cited Eisenhart papers; and Arscott's 1963 paper. Source material supplied by the author, including physical-copy photographs, was used for these comparisons, alongside the cited scans. The general-theory appendices are based on the cited Moon–Spencer, Morse–Feshbach, Stäckel and Eisenhart sources. The p. 45 Laplacian typography was checked against the copies of Moon and Spencer's handbook consulted for this note, including the corrected third printing (Springer, 1988). Responsibility for the final text and its verification remains with the author.

References

[1] P. Moon and D. E. Spencer, *Field Theory Handbook*, 2nd ed. (Springer, 1971), corrected third printing (1988), ISBN 0-387-18430-9 (printing checked), pp. 1–9 and Table 1.11, pp. 44–48.

[2] P. M. Morse and H. Feshbach, *Methods of Theoretical Physics*, Part I (McGraw-Hill, New York, 1953; reprinted by Feshbach Publishing, Minneapolis, ISBN 0-9762021-0-7), pp. 655–656, 664–665. Pages 655–656 and 664 were checked in the Feshbach Publishing reprint; pp. 664–665 also in the McGraw-Hill printing.

[3] L. P. Eisenhart, Separable systems of Stäckel, *Ann. of Math.* (2) **35** (1934), no. 2, 284–305, doi:10.2307/1968433.

[4] L. P. Eisenhart, Separable systems in Euclidean 3-space, *Phys. Rev.* **45** (1934), no. 6, 427–428, doi:10.1103/PhysRev.45.427.2.

[5] L. P. Eisenhart, Enumeration of potentials for which one-particle Schrödinger equations are separable, *Phys. Rev.* **74** (1948), no. 1, 87–89, doi:10.1103/PhysRev.74.87.

[6] P. Stäckel, *Über die Integration der Hamilton-Jacobischen Differentialgleichung mittelst Separation der Variabeln*, Habilitationsschrift, Halle, 1891.

[7] J. R. Philip and J. H. Knight, Table Errata 609 [P. Moon and D. E. Spencer, *Field Theory Handbook*, 2nd ed., Springer, 1971], *Math. Comp.* **49** (1987), no. 180, 651–653, doi:10.1090/S0025-5718-87-99755-9.

[8] M. Willatzen and L. C. Lew Yan Voon, *Separable Boundary-Value Problems in Physics* (Wiley-VCH, Weinheim, 2011), ISBN 978-3-527-41020-0, Table 2.1, p. 18, and Ch. 17, pp. 217–229.

[9] L. Duggen, M. Willatzen and L. C. Lew Yan Voon, Laplace boundary-value problem in paraboloidal coordinates, *Eur. J. Phys.* **33** (2012), no. 3, 689–696, doi:10.1088/0143-0807/33/3/689.

[10] G. Arfken, *Mathematical Methods for Physicists*, 2nd ed. (Academic Press, 1970), §2.17, "Confocal Parabolic Coordinates," pp. 119–120.

[11] G. B. Arfken, H. J. Weber and F. E. Harris, *Mathematical Methods for Physicists*, 7th ed. (Academic Press, 2013), §3.10 and p. 203.

[12] E. W. Weisstein, "Confocal Paraboloidal Coordinates," *MathWorld—A Wolfram Web Resource*, `https://mathworld.wolfram.com/ConfocalParaboloidalCoordinates.html` (accessed 7 November 2026).

[13] F. M. Arscott, Paraboloidal co-ordinates and Laplace's equation, *Proc. Roy. Soc. Edinburgh Sect. A* **66** (1962–63), 129–139 (issued 30 May 1964), doi:10.1017/S0080454100007780.

[14] F. M. Arscott, The Whittaker–Hill equation and the wave equation in paraboloidal co-ordinates, *Proc. Roy. Soc. Edinburgh Sect. A* **67** (1967), no. 4, 265–276, doi:10.1017/S008045410000813X.

[15] F. M. Arscott, *Periodic Differential Equations*, Int. Ser. Monographs Pure Appl. Math. **66** (Pergamon, 1964), §1.1, p. 2, doi:10.1016/C2013-0-01721-5.

[16] C. P. Boyer, E. G. Kalnins and W. Miller Jr., Symmetry and separation of variables for the Helmholtz and Laplace equations, *Nagoya Math. J.* **60** (1976), 35–80, doi:10.1017/S0027763000017165.

[17] W. Miller, Jr., *Symmetry and Separation of Variables*, Encyclopedia of Mathematics and Its Applications, Vol. 4 (Addison-Wesley, Reading, MA, 1977), ISBN 0-201-13503-5, Chapter 3, §§3.1 and 3.6.

[18] A. Darai and F. M. Arscott, A three-dimensional parabolic punch problem in linear elasticity, *J. Engrg. Math.* **24** (1990), 369–383, doi:10.1007/BF00130689.

[19] A. Darai, *Applications of Higher Special Functions to Some Three-Dimensional Contact Problems in the Classical Theory of Elasticity*, Ph.D. thesis, University of Manitoba (1985), Ch. 3, `http://hdl.handle.net/1993/29014`.

[20] N. W. McLachlan, *Theory and Application of Mathieu Functions* (Oxford University Press, 1947), §§2.151, 8.14, 8.30, 10.50–10.51 and 11.12.

[21] D. H. Armitage and S. J. Gardiner, *Classical Potential Theory*, Springer Monographs in Mathematics (Springer-Verlag London, 2001), ISBN 978-1-4471-1116-0, doi:10.1007/978-1-4471-0233-5.

[22] U. G. Abdulla and D. Brazke, The Wiener criterion at ∞ for degenerate elliptic equations, arXiv:2510.15249 (2025).

[23] N. N. Lebedev, *Special Functions and Their Applications*, revised English ed., transl. and ed. R. A. Silverman (Prentice-Hall, Englewood Cliffs, NJ, 1965).

[24] N. N. Lebedev, I. P. Skalskaya and Y. S. Uflyand, *Worked Problems in Applied Mathematics*, transl. R. A. Silverman (Dover, New York, 1965), pp. 231–233.

[25] F. W. J. Olver, A. B. Olde Daalhuis, D. W. Lozier, B. I. Schneider, R. F. Boisvert, C. W. Clark, B. R. Miller, B. V. Saunders, H. S. Cohl and M. A. McClain (eds.), *NIST Digital Library of Mathematical Functions*, Release 1.2.8 of 2026-09-15, `https://dlmf.nist.gov/`; equation numbers cited are those of this release.